Legates David R (Orcid ID: 0000-0003-4323-4416)

Confidential manuscript submitted to the International Journal of Climatology

# Detection of Climate Transitions and Discontinuities by Hurst Rescaling

## Short Title: Detection of Climate Transitions/Discontinuities by Hurst Rescaling

**David R. Legates[1] and Samuel I. Outcalt[2]**

[1]College of Earth, Ocean, and Environment, University of Delaware, Newark DE 19716 USA.

[2]Emeritus Professor of Physical Geography, University of Michigan, Ann Arbor MI 48109 USA.

Corresponding author: David R. Legates (legates@udel.edu), 216 Pearson Hall, 125 Academy Street, Department of Geography and Spatial Sciences, University of Delaware, Newark DE 19716-2514. Phone: 1-302-831-4920; Fax: 1-302-831-6654.

**Abstract**

The method of Outcalt *et al.* (1997), based on work developed originally by Hurst (1951; 1956), is reexamined to evaluate its efficacy in delineating changes in trends and identifying regime shifts in climatic-related time series. This technique is based on the concept of the normalized rescaled running sum where temporal changes in the Hurst exponent can be used to identify climatic trends from one regime to another as each regime has a characteristic distribution that differs from the statistical characteristics of the complete time series. An examination of the temporal change in the amplitude of the normalized rescaled running sum can be used as a method to identify these regime changes, which may be either real (*i.e.*, a true climatic shift) or induced (*i.e.*, through a change in measurement bias, station location, or other non-climatic influence). Examples shown here focus on examining time series of the Pacific Decadal Oscillation, Arctic thaw depth, the Northern Hemisphere snow cover extent, treeflow data from Lees Ferry (AZ), North Atlantic tropical cyclone frequency, and central England air temperatures.

**Key Words:** Hurst rescaling, Integral trace, Normalized Rescaled Running Sum, Arctic thaw depth, central England air temperatures, North Atlantic tropical cyclone frequency, Northern Hemisphere snow cover extent, Pacific Decadal Oscillation, Treeflow

## 1 Introduction

Hurst (1951; 1956) discovered that measurements of numerous geophysical time series demonstrate the presence of long-range dependence, which had earlier been described in the analysis of turbulence by Kolmogorov (see Koutsoyiannis *et al.,* 2008). Investigating fluctuations in annual water level for the Nile River in Egypt, Hurst (1951; 1956) found that the river exhibited a peculiar long-term behavior: years of drought are more likely followed by another drought year than a year of flooding and vice versa. Such behavior does not conform to the standard assumption of independence – the absence of a temporal autocorrelation – but rather, a system "memory" appears to exist that lies outside traditional atmospheric dynamic forcings (Koutsoyiannis and Montanari, 2015). Local shifts in the mean are expected behavior under an assumption of persistence, which is widely seen in climatic time series (Koutsoyiannis, 2013).

In statistical terminology, the behavior of the annual Nile River flow exhibited fewer runs of anomalously high and low flows than if fluctuations were random (Barton and David, 1957). In this context, a run is composed of consecutive outcomes (high or low flow) that occur sequentially. If the data were truly random, then the expected number of runs (*i.e.*, the mean) would be (Barton and David, 1957)

$$E[\mu] = \frac{2\ N^+ N^-}{N} + 1 \tag{1}$$

with a variance of

$$E[\sigma^2] = \frac{2\ N^+ N^- \left(2\ N^+ N^- - N\right)}{N^2\ (N-1)} \tag{2}$$

where $N$ is the number of observations (i.e., the length of the time series), $N^+$ is the number of sequences for which the values were above the mean and $N^-$ is the number of sequences for which the values were below the mean ($N = N^+ + N^-$). If the number of runs is greater than the

expected value, negative temporal autocorrelation exists (*i.e.*, high values are more likely followed by a value below the mean while low values are more likely followed by values above the mean). Conversely, if the number of runs is less than the expected value, then positive temporal autocorrelation exists (*i.e.*, higher values are more likely followed by another high value while low values are more likely followed by another low value). Consistent with Hurst's findings, positive temporal autocorrelation produces a time series that exhibits more lower frequency variability and less higher frequency variability than would be expected if the time series were a truly random process and stationary in the mean (see Figure 1). This increase in lower frequencies often is mischaracterized as a "fat-tailed" (or heavy-tailed) distribution even though many of the processes are still Gaussian, which explicitly excludes fat tails (see Koutsoyiannis, 2005a, b).

Interestingly, Hurst and later researchers have found that numerous other physical variables tend to exhibit positive temporal autocorrelation "memory". Sutcliffe *et al.* (2016) provides documentation that Hurst's analysis had been extended to cover 75 different phenomena, including river statistics, rainfall, air temperature and pressure, tree rings, sunspot numbers, wheat prices, and varves in Canada, Norway, and Lake Saki (Crimea) (see their Figure 5). Indeed, this process has now been recognized as an innovative application of natural fractal geometry (Mandelbrot 1982) and has been widely used as a technique of time-series analysis.

This paper revisits the Hurst-Kolmogorov process and, specifically, the *integral trace* or the *normalized rescaled running sum*, as it is alternatively called (Outcalt *et al.,* 1997). The integral trace allows intercomparison of variables with different metrics, is independent of the start or end of the period of record and is unusually robust (Outcalt *et al.,* 1997; Runnalls and Oke, 2006). For example, the Budyko Hypothesis (Budyko, 1948) has been used to analyze regional differences in long-term annual water and energy balance time series to identify the influence of

changes on mean annual runoff and evapotranspiration. Hurst rescaling can be used to examine how changes in streamflow can be explained by variability in precipitation and evapotranspiration (see Istanbulluoglu *et al.*, 2012; Niu *et al.* 2021).

Although it is not a new method, the integral trace has several features that make it an important and underutilized method. Moreover, this paper defines how a modification of it can be used in climatological settings to detect climate shifts from natural causes, anthropogenic changes, or observational biases. The method has been used successfully in a variety of different settings including air temperature thresholds in an urban setting (Ruddell *et al.,* 2013), an evaluation of turbulent flows (van Atta and Helland, 1977), land-use-dependent surface thermal contrasts (Outcalt, 1972; Pease *et al.,* 1976), natural terrain texture (Outcalt and Melton, 1992), warming of the active layer (Hinkel and Outcalt, 1995), and water-/lake-level variation (Kenkel, 1995; Todhunter, 2012; Todhunter and Fietzek-DeVries, 2016). Moreover, the integral trace has been used successfully to detect microclimatic inhomogeneities in air temperature data (Runnalls and Oke, 2006) and atmospheric turbulence (Dias *et al.,* 2018). Several atmospheric-related applications will be shown here to illustrate the utility of the method. It is suggested the reader

consult Cohn and Lins (2005), Koutsoyiannis and Cohn (2008), O'Connell *et al.* (2016), and Koutsoyiannis *et al.* (2018) for a deeper discussion of Hurst-Kolmogorov statistics.

## 2 The Hurst Exponent

Hurst (1951; 1956) determined that for a time series, $\boldsymbol{X_t}$, of length $\boldsymbol{n}$ (*i.e.*, $\boldsymbol{t} = [\mathbf{1}, \boldsymbol{n}]$),

$$\frac{\boldsymbol{R(n)}}{\boldsymbol{S(n)}} \propto \boldsymbol{n^H} \tag{3}$$

where $\boldsymbol{R(n)}$ is its *adjusted range*, given by $[\mathbf{max}(\boldsymbol{x_t}) - \mathbf{min}(\boldsymbol{x_t})]\ \forall\ \boldsymbol{t}$, $\boldsymbol{S(n)}$ is the standard deviation of the time series, and $\boldsymbol{H}$ is the *Hurst exponent*. To calculate $\boldsymbol{H}$, all subsets of the time series of length $(\boldsymbol{n} - \boldsymbol{i})$, where $\boldsymbol{i} = [\mathbf{0}, \boldsymbol{n} - \mathbf{1}]$, are used to compute the *rescaled range*, $\boldsymbol{RR(n)}$,

$$\boldsymbol{RR(n)} = \mathbf{ln}\left[\frac{\boldsymbol{R(n)}}{\boldsymbol{S(n)}}\right] \quad . \tag{4}$$

The rescaled range is the amplitude of the integral trace of deviations from the mean of the time series. Moreover, the slope of the logarithm of the rescaled range plotted versus the logarithm of $\boldsymbol{n}$ is $\boldsymbol{H}$ (Equation 3). Note that this derivation is consistent with Schroeder (1991) rather than using the logarithm of the ratio of $\boldsymbol{n}$ to $\boldsymbol{S(n)}$ as the abscissa (see Potter, 1979 and Outcalt *et al*., 1997). For additional discussion on the rescaled range, see Hamed (2007) and Ceballos and Largo (2017). Moreover, this method is similar to the normalized dynamic range presented by Wu *et al.* (2021).

If the time series is a truly random sample taken from a Gaussian distribution, $\boldsymbol{H}$ would be 0.5 and spectral distribution would represent Brownian noise (sometimes called Brown noise or red noise) – the amplitude of the frequencies produced by Brownian motion or a random walk process (see Santana and Coelho, 2012). True Brownian noise will decrease by 20 dB per $\log_{10}$ of the frequency; thus, it is dominated by lower frequencies. But Hurst noticed, as have many subsequent researchers, that the value of $\boldsymbol{H}$ usually exceeds 0.5 and is often between 0.6 and 0.9

for many geophysical time series. This implies that these time series exhibit a higher degree of temporal autocorrelation than would be expected from a purely random process. An extreme value of 1.0 for ***H*** often is referred to as black noise (Outcalt *et al.,* 1997).

Several researchers have argued that a Hurst exponent exceeding 0.5 results from the fact that while the entire time series may be stationary, certain sub-periods are not. Thus, the time series exhibits a shifting mean at time-scales shorter than the record length (Wallis and O'Connell, 1973; Klemeš, 1974; Potter, 1976; Boes and Salas, 1978; Potter, 1979; Mesa and Poveda, 1993). The concept behind Hurst rescaling is that if the process is consistent in time; that is, the Brownian motion/random walk process remains constant across the entire time series, the mean value of ***H*** will remain largely constant over time. However, if the process changes over the duration of the time series, this would be reflected in a temporal change in ***H***. This paper argues that an examination of the temporal change in the amplitude of the rescaled range (*i.e*., the integral trace) can be used as a method to identify changes in climate regimes or measurement discontinuities, such as station relocations and instrumentation changes.

The Hurst process has an interesting interpretation when considering turbulence and Brownian motion. Nordin *et al.* (1972) argue that for Hurst phenomenon, the integral scale can be considered infinite and thus, a diffusing particle moving with Brownian motion can be modeled as a fractal dimension. Fischer (1973) suggested some of this behavior could be explained as secondary flow resulting from edge effects or other interfering properties. Moreover, the turbulent velocity would be a continuous Gaussian noise process, albeit fractional. For more discussion, see Nordin *et al.* (1972), Fischer (1973), and van Atta and Helland (1977).

It should be noted that the traditional description of the Hurst process using the rescaled range is somewhat outdated. Although it has historical roots and provides an effective way to

understand the process, Koutsoyiannis (2002) demonstrates that the rescaled range exhibits more bias and a higher degree of uncertainty than the variance of the time-averaged process. Thus, Koutsoyiannis suggests the *climacogram* as a more intuitive alternative (see also Dimitriadis and Koutsoyiannis, 2015).

The climacogram is a logarithmic plot of the variance of a time series, $\boldsymbol{\gamma_k^2}$, averaged over time scale $\boldsymbol{k}$ versus $\boldsymbol{k}$ (Koutsoyiannis *et al.,* 2018). The time scale $\boldsymbol{k}$ is computed for integer values of $\boldsymbol{k} = [\mathbf{1}, \boldsymbol{k_{max}}], \boldsymbol{k_{max}} \leq \mathbf{0.1}\, \boldsymbol{n}$ where $\boldsymbol{n}$ is the length of the time series. For $\boldsymbol{k} = \mathbf{1}$, each of the values of the time series are taken individually; thus, $\boldsymbol{\gamma_1^2}$ is simply the variance in the time series. For $\boldsymbol{k} = \mathbf{2}$, the values are paired (1 with 2, 3 with 4, *etc.*), averaged, and the variance of their averages constitute $\boldsymbol{\gamma_2^2}$. Similarly, the calculation of $\boldsymbol{\gamma_k^2}$ proceeds through $\boldsymbol{k} = \boldsymbol{k_{max}}$. From the slope ($\boldsymbol{b}$) of the line ($\boldsymbol{\gamma_k^2}$ versus $\boldsymbol{k}$), the Hurst parameter ($\boldsymbol{H}$) is computed using $\boldsymbol{H} = \frac{\mathbf{1}}{\mathbf{2}}(\boldsymbol{b} + \mathbf{2})$. Although potentially exhibiting more bias and error variance, the rescaled range will be used in the remainder of this manuscript instead of the climacogram, as the original derivation by Outcalt *et al.* (1997) utilized the rescaled range and consistency with earlier uses of the integral trace is desired. Subsequent research will focus on upgrading the method by using the climacogram.

It should be noted that the use of the integral trace lends itself to several areas of scientific inquiry. In particular, the integral trace can be used (1) to identify natural regime changes in a variable, (2) to examine regime changes from known external forcings, (3) to examine regime changes resulting from suspected discontinuities in the time series, and (4) to identify both the timing (*i.e.*, from transitions between ascending and descending traces) and the magnitude of

regime changes (*i.e.*, as determined by the amplitude of the traces). Thus, the integral trace may be used as both a diagnostic tool and as a confirmatory tool.

## 3 Method

### *3.1 Integral Trace*

Using the Hurst-Kolmogorov process, Outcalt *et al*. (1997) determined that patterns in the integral trace can identify regime changes or measurement discontinuities in the time series. These patterns could make such identifications in cases where tests of discontinuities in the bulk data failed. Differences in the patterns of the temporal autocorrelation were useful to make these identifications.

The method is based on Hurst rescaling and proceeds as follows from Outcalt *et al.* (1997). First, the grand mean is subtracted from each observation and these mean deviations are added together to produce a running sum for each observation (column C in the supplementary material). Because the sum of all mean deviations must equal zero, the last observation has a running sum of zero. The normalized rescaled running sum then is computed by taking the running sum for each observation, subtracting the minimum accumulated deviation, and then dividing by the range of the accumulated deviations (column D in the supplementary material). The rescaled range then is computed by taking the range of the deviations from the mean and dividing by the standard deviation of the original observations (in this case, the sample standard deviation, with $\boldsymbol{n-1}$ in the denominator, should be used). Finally, the Hurst Exponent is computed by taking the ratio of the natural log of the rescaled range (or the natural log of the range of the accumulated deviations divided by the standard deviation of the observations) and dividing by the natural log of the number of observations (Schroeder, 1991). The normalized observation also can be computed by

subtracting the minimum value from the original observations and dividing by the range (column E in the supplementary material).

Next, the minimum of the deviations from the mean is subtracted from each deviation from the mean ($\boldsymbol{min}[\boldsymbol{x_t} - \overline{\boldsymbol{x}}]$) and the result is divided by their range to produce the normalized rescaled running sum. The normalized rescaled running sum can be plotted as a function of time to produce the integral trace (Outcalt *et al.,* 1997). This integral trace is used to screen for changes in the character of the time series, although we caution against interpretation of every small deviation in the integral trace (see Klemeš, 1986). If desired, the observations can be normalized by removing the mean and then dividing by the range, to create a series that ranges from zero to one. Normalizing the observations allows for the raw and rescaled data to be easily intercompared (Outcalt *et al.,* 1997; see also Runnalls and Oke, 2006).

*3.2 A Simple Example*

A simple example with known characteristics *á priori* would be helpful. Consider a time series (Table 1) with $\boldsymbol{n = 50}$. In this example, the observations, $\boldsymbol{X_t}$, are taken from a Gaussian normal distribution. However, for $\boldsymbol{t = [1, 15]}$, the population mean is 20.0 and its standard deviation is 2.0 ($\boldsymbol{N(20, 2)}$), for $\boldsymbol{t = [16, 34]}$, the population mean is 22.0 and its standard deviation is 2.0 ($\boldsymbol{N(22, 2)}$), and for $\boldsymbol{t = [35, 50]}$, the population mean is 22.0 and its standard deviation is 3.0 ($\boldsymbol{N(22, 4)}$). Thus, between $\boldsymbol{t = 15}$ and $\boldsymbol{t = 16}$, a change in the mean occurs while between $\boldsymbol{t = 34}$ and $\boldsymbol{t = 35}$, a change in the standard deviation occurs. The Hurst exponent, $\boldsymbol{H}$, for the entire time series is 0.6292 (Table 1), implying the presence of Hurst-Kolmogorov behavior

(or long-term dependence). However, it changes due to the inherent discontinuities in the time series.

Visually, it is difficult to assess the known changes in the mean and standard deviation from even a close examination of the original data (Figure 2a). Although a shift in the mean occurs at $\boldsymbol{t = 15/16}$, it is not apparent on the graph; neither is the shift in the standard deviation at $\boldsymbol{t = 34/35}$. In fact, the data might be visually interpreted as heteroscedastic with an increasing trend over the entire time series and an increasing standard deviation over the entire time domain.

The underlying signal becomes more obvious when the normalized rescaled running sum is plotted as a function of time (Figure 2b). The graph shows a steady decline until between $\boldsymbol{t = 15}$ and $\boldsymbol{t = 18}$ with a near constant slope. Then, the slope becomes near zero until about $\boldsymbol{t = 34}$ when it dramatically increases for the remainder of the time series. It may be difficult to pinpoint exactly when the underlying signal changes; however, three regimes clearly exist and are properly identified, which captures the pattern inherent in the original data successfully. Nevertheless, both the change in mean and the change in variance (heteroscedasticity) were identified properly.

To assess whether the apparent change in slope is statistically significant between any of these regions, parametric or non-parametric tests can be employed. For example, Welch's parametric test (Andrade and Estévez-Pérez, 2014) can be used because it does not *á priori* assume that the population variances of the two samples are equal, although several other alternatives have been utilized (*cf.*, Chow, 1960; Hjellvik and Tjøstheim, 1995). The Mann-Kendall test is the most often used non-parametric test although other alternatives do exist (*cf.*, Sen, 1965; Hjellvik and Tjøstheim, 1995). Choices usually are made based on the length of the time series and the non-normality/presence of outliers with preference to parametric tests given to longer time series and absence of non-normality and outliers (*cf.,* Fagerland, 2012). Parametric solutions require more

assumptions while the tradeoff is a lack of power associated with non-parametric solutions (Yue *et al.,* 2002). However, only a physical reason or suspected breakpoint warrants testing, as Type I errors may result when testing multiple hypotheses (see Nakagawa and Cuthill, 2007; Clarke, 2010). Moreover, the use of both hypothesis testing and *p*-values has been questioned with alternatives proposed (see Briggs, 2017; 2019; McShane and Gal, 2017; Briggs *et al.,* 2019; Halsey, 2019; Wasserstein *et al.,* 2019).

For illustrative purposes only, the Walsh test will be used here with this simple example. Its test statistic is given by

$$\boldsymbol{t} = \frac{(\boldsymbol{b_1} - \boldsymbol{b_2})}{\sqrt{\frac{\boldsymbol{s^2_{(y|x)1}}}{\Sigma(\boldsymbol{x_{i1}} - \bar{\boldsymbol{x}}_{\boldsymbol{1}})^{\boldsymbol{2}}} + \frac{\boldsymbol{s^2_{(y|x)2}}}{\Sigma(\boldsymbol{x_{i2}} - \bar{\boldsymbol{x}}_{\boldsymbol{2}})^{\boldsymbol{2}}}}} \tag{5}$$

with

$$\boldsymbol{\gamma} = \frac{\left[\frac{\boldsymbol{s^2_{(y|x)1}}}{\Sigma(\boldsymbol{x_{i1}} - \bar{\boldsymbol{x}}_{\boldsymbol{1}})^{\boldsymbol{2}}} + \frac{\boldsymbol{s^2_{(y|x)2}}}{\Sigma(\boldsymbol{x_{i2}} - \bar{\boldsymbol{x}}_{\boldsymbol{2}})^{\boldsymbol{2}}}\right]^{\boldsymbol{2}}}{\boldsymbol{n_1^{-1}}\left[\frac{\boldsymbol{s^2_{(y|x)1}}}{\Sigma(\boldsymbol{x_{i1}} - \bar{\boldsymbol{x}}_{\boldsymbol{1}})^{\boldsymbol{2}}}\right]^{\boldsymbol{2}} + \boldsymbol{n_2^{-1}}\left[\frac{\boldsymbol{s^2_{(y|x)2}}}{\Sigma(\boldsymbol{x_{i2}} - \bar{\boldsymbol{x}}_{\boldsymbol{2}})^{\boldsymbol{2}}}\right]^{\boldsymbol{2}}} \tag{6}$$

degrees of freedom where $\boldsymbol{b}$ is the slope, the overbar denotes the mean, $\boldsymbol{s^2_{(y|x)}}$ is the square of the standard error of the slope (the variance of the errors about the regression line), and the subscripts $\mathbf{1}$ and $\mathbf{2}$ denote the two potentially disparate time series. The null hypothesis is that the differences in the population slopes are zero (i.e., $\boldsymbol{\beta_1} = \boldsymbol{\beta_2}$ or $\boldsymbol{\beta_1} - \boldsymbol{\beta_2} = \mathbf{0}$) with the alternative hypothesis that they are not zero (i.e., $\boldsymbol{\beta_1} \neq \boldsymbol{\beta_2}$ or $\boldsymbol{\beta_1} - \boldsymbol{\beta_2} \neq \mathbf{0}$).

First, consider the comparison of the slope of the time series between $\boldsymbol{t} = [\mathbf{1}, \mathbf{15}]$ (subscript 1) and $\boldsymbol{t} = [\mathbf{16}, \mathbf{34}]$ (subscript 2) for the normalized rescaled running sum (Figure 2b). The means are 0.51 and 0.19, the slopes are -0.058 and 0.0016, and the squares of the standard

error of the estimate are 0.0029 and 0.0034, for the two time-series segments, respectively. This yields a $\boldsymbol{t}$-statistic of -14.68 (i.e., $\boldsymbol{\beta_1 < \beta_2}$) with 30 degrees of freedom ($\boldsymbol{\gamma = 29.68}$), which is statistically significant at $\boldsymbol{\alpha < 0.01}$. Thus, it can be concluded that the slopes for the time segments between $\boldsymbol{t = [1, 15]}$ and $\boldsymbol{t = [16, 34]}$ are statistically different, which implies that a shift in the population statistics exists between time 15 and 16. One could search for a smaller *p*-value by comparing $\boldsymbol{t = [1, 14]}$ and $\boldsymbol{t = [15, 34]}$ or comparing $\boldsymbol{t = [1, 16]}$ and $\boldsymbol{t = [17, 34]}$ if it were not known exactly where the discontinuity occurred (as is often the case in an operational setting), for example.

Similarly, for the comparison between the second time segment ($\boldsymbol{t = [16, 34]}$) and the third time segment ($\boldsymbol{t = [35, 50]}$), the $\boldsymbol{t}$-statistic is -8.04 (i.e., $\boldsymbol{\beta_2 < \beta_3}$) with 21 degrees of freedom ($\boldsymbol{\gamma = 20.90}$) which is also statistically significant at $\boldsymbol{\alpha < 0.01}$. Thus, it can be concluded that the Hurst rescaling method can clearly detect changes in both the first (mean) and second (variance) moments of this illustrative distribution.

## 4 Real World Examples

To demonstrate the efficacy of the Hurst rescaling method, six disparate, real-world datasets are examined. These datasets are chosen largely to highlight known discontinuities in a time series to establish whether the method can indeed find discontinuities that have already been identified, thereby providing a fair evaluation of the veracity of the methodology. These examples demonstrate how the integral trace can be used in the four applications (to identify natural regime changes in a variable, to examine regime changes from known external forcings, to examine regime changes resulting from suspected discontinuities in the time series, and to identify both the timing and the magnitude of regime changes).

*4.1 The Pacific Decadal Oscillation*

This example uses the integral trace to examine regime changes due to known natural climate forcings – the Pacific Decadal Oscillation (PDO) – and highlights the match between the timing and number of regime shifts evident in the trace and the changes in PDO noted in the literature.

The PDO is defined as variability in the sea surface temperatures of the Pacific Ocean that lasts for multiple decades (Mantua *et al.,* 1997; Zhang *et al.,* 1997). Specifically, it is represented by the first principal component (or empirical orthogonal function, EOF) of sea surface temperature (SST) anomalies (with both the global mean SST anomaly and the annual cycle removed) in the North Pacific Ocean (*i.e.*, poleward of 20°N). A positive value of the PDO corresponds with negative SST anomalies in the central and western North Pacific and positive anomalies in the eastern tropical Pacific while a negative value for the PDO generally reverses this pattern. Shifts in the PDO are linked to changes in air temperature patterns over land areas in the North Pacific region (Johnstone and Mantua, 2014; Khapalova *et al.,* 2018), fluctuations in tropical cyclone activity in both the Atlantic and Pacific basins (Lupo *et al.,* 2008, Kubota and Chan, 2009), the occurrence of droughts and floods around the Pacific Rim (McCabe *et al.,* 2004; Zhou and Liu, 2018), and changes in the productivity of marine ecosystems (Litzow *et al.,* 2020), for example.

The PDO has been linked to the *Great Pacific Climate Shift*, which occurred during the winter of 1976/1977. This change in SSTs and the PDO has been well-documented (*e.g.*, Hurrell and van Loon, 1994; Miller *et al.,* 1994; Gedalof and Smith, 2001; Giese *et al.,* 2001; Hartmann and Wendler, 2005; Meehl *et al.,* 2009; Swanson and Tsonis, 2009; Khaliq and Gachon, 2010; Ding *et al.*, 2013) and is associated with concomitant changes in atmospheric circulation. A

deepening of the Aleutian Low shifted storm tracks to the south and increased their intensity. Over North America, air temperatures increased in the northwest while storminess decreased in the southeast. Even Pacific Ocean ecosystems were affected (see Venrick *et al*., 1987, Polovina *et al.,* 1994). Other major shifts in the PDO occurred in approximately 1947 and 1999 (concomitant with the major El Niño event of the given year). More recently, the PDO has fluctuated on a much faster time scale with changes occurring in 2002, 2007, and 2014 (Bond *et al*., 2003; Ding *et al.*, 2013; Bond *et al.,* 2015; Hartmann, 2015).

Monthly data for the PDO from January 1900 to September 2018 were obtained from Nate Mantua's Anonymous FTP directory (*http://research.jisao.washington.edu/pdo/PDO.latest.txt* accessed on September 2, 2021). Considerable monthly variability exists in the data and the Great Pacific Climate Shift is not obvious from visual inspection (Figure 3a). The plot of the normalized rescaled running sum (Figure 3b), however, shows clearly that two major shifts occurred – one in May 1943 and the other in May 1976. Both have been extensively documented as major shifts in the PDO (see Hidalgo and Dracup, 2003). Moreover, Welch's test on the normalized rescaled running sum also suggests four changes between 1998 and 2014 (Figure 3b) although we do suggest that caution be exercised in overemphasizing short-term fluctuations in the normalized rescaled running sum. Nevertheless, the normalized rescaled running sum identifies transitions that occurred in June 1998, July 2002, July 2006, and March 2013. These temporal changes in the PDO also are identified by Bond *et al.* (2003; 2015), Ding *et al.* (2013), and Hartmann (2015).

*4.2 Thaw Depth in Northern Alaska*

Nelson *et al*. (1998) documented a radical shift in the relationship between the depth of summer thaw and the degree days of thaw using early records taken by the United States Army

Cold Regions Research and Engineering Laboratory (CRREL) between 1962 and 1966 and resumed observations beginning in 1991 or 1992. This dramatic shift can be considered a response to the 1976 global climate transition in PDO discussed previously (Section 4.1, see Hartmann and Wendler, 2005). Evidence also exists that permafrost temperatures can be linked to solar variability (Osterkamp *et al*., 1994; Overpeck *et al*., 1997). Thus, this example uses the integral trace to identify natural regime changes in a climate variable.

Mean thaw depth for four CALM grids in Arctic Alaska – West Dock, Betty Pingo, Happy Valley, and Imnavait Creek – from 1992 to 2018 were used to investigate the impact of solar regime changes on thaw in northern Alaska detected in the early 21$^{st}$ century (Figure 4a – Outcalt, 2018). These locations represent a transect along the Sag River from its outlet at Prudhoe Bay to interior Alaska. West Dock is located along the coast and Betty Pingo is located about 50 km inland. Happy Valley and Imnavait Creek are located much farther inland – approximately 400 km and 550 km, respectively (see Streletskiy *et al.,* 2008).

Two strong inflection points are indicated by the normalized rescaled running sum (Figure 4b) using Welch's test. The first inflection point occurs in 1998 for all stations except Imnavait Creek. It is possible that the change at Imnavait Creek occurred earlier (1994 is implied by the graph although the time series is sparse before 1994). A second inflection is identified at 2007-2008 at Happy Valley and Imnavait Creek and in 2010 at West Dock and Betty Pingo. It is

possible that the change occurred first in the north (possibly moderated by the Arctic Ocean) and was delayed by a couple of years for the inland stations.

*4.3 Northern Hemisphere Snow Cover*

This example compares an integral trace obtained from one set of imagery (*i.e.*, snow cover) and comparing them to another example from the literature using a different variable (*i.e.,* snow water equivalent) and imagery.

Monthly Northern Hemisphere snow cover data were obtained from the Rutgers University Global Snow Lab (*https://climate.rutgers.edu/snowcover/files/moncov.nhland.txt*, downloaded on April 20, 2019) from October 1971 to March 2019. These data are based on maps of snow and ice areas produced by the US National Oceanic and Atmospheric Administration (NOAA) using visual interpretation of shortwave imagery. Spatial resolution changed from about 4 km to 1 km with imagery from more advanced satellites in 1972; before this period, snow extent was generally underestimated. For more information on how these data were compiled, see Robinson *et al.* (1993; 2012) and Estilow *et al*. (2015). Before calculating the normalized rescaled running sum, the data were detrended by removing the 48-year average monthly snow cover from the monthly values to produce a seasonally-detrended time series.

Monthly snow cover data for the Northern Hemisphere (Figure 5a) show considerable monthly variability, particularly so in the early and late portions of the record. This change in variability is exhibited in a change in the normalized rescaled running sum (Figure 5b) in mid-1979 and early 2005, as identified using Welch's test. In addition, there are major inflection points

in mid-1987 and early 1995, which are concomitant with shifts in the monthly trends of snow cover (Figure 5a).

The change between mid-1979 and early 2005 also is identified by Gan *et al.* (2013) who used satellite data (surface brightness temperature) to evaluate North American snow water equivalent. Their negative trend began in 1979, reached a minimum in April of 2005 and, according to Gan *et al.* (2013), the pattern ended in 2007 and is linked to an overall decrease in rising air temperatures in high latitudes; this is consistent with the finding using Hurst rescaling (Figure 5b).

*4.4 Treeflow Records from Lees Ferry, Arizona*

Treeflow records (*i.e.*, streamflow reconstructions from tree rings) can be inferred using a linear regression between tree-ring data and observed stream flow/discharge. This regression then is used to estimate the discharge for the length of the tree-ring record (see Meko *et al*., 2007; Mauget, 2015). These treeflow records are based on tree species that reliably have been proven to estimate observed streamflow; tree growth in more arid environments (such as the western United States) are more responsive to variability in moisture conditions, thereby providing a reasonable approximation to the hydroclimatological conditions that exist. The regression then is used to extend the record prior to the gauged record using the tree rings as surrogates for the observations. To refine the streamflow reconstruction, multiple trees (20 to 40) are employed so that the treeflow records are not influenced by peculiarities associated with a single tree (Rice *et al*., 2009, Treeflow, 2019).

For this analysis, treeflow data were obtained for Lees Ferry, Arizona, located just downstream from the Glen Canyon Dam that forms Lake Powell (and near the Colorado state line)

and is the demarcation between the Upper and the Lower Colorado River Basins (Outcalt, 2015). A stream gauge was installed at Lees Ferry in 1921 but over time, the natural flow of the Colorado River has been affected by human activities in the Upper Colorado River Basin. Adjustments have been made to the gauge record to account for water diversions in the Upper Colorado River Basin and changes to the stream channel that have created increased evaporative losses. Construction of the Glen Canyon Dam began in 1960, which further affected streamflow at Lees Ferry (Cech, 2009).

Streamflow reconstructions were accomplished by calculating treeflow parameters to allow for the altered flow produced by the dam and other human-induced effects. The treeflow record at Lees Ferry is displayed (Figure 6a) and provides a reconstruction of streamflow using tree-ring chronologies from 762 to 2005 AD. For a more complete discussion of how the Lees Ferry treeflow reconstruction was calibrated, see Meko *et al*. (2007) and Mauget (2015).

The normalized rescaled running sum (Figure 6b) shows a strong change (large inflections) in the streamflow regime corresponding to the beginning of the Medieval Warm Period (*i.e*., the early 11$^{th}$ century) as well as the beginning (*i.e*., the early 14$^{th}$ century) and end (*i.e*., the mid-19$^{th}$ century) of the Little Ice Age. A closer examination of the normalized rescaled running sum from 1965 to 2005 shows a minimum in 1977. The minimum is commensurate with the Great Pacific Climate Shift discussed earlier while the second is commensurate with the global warming hiatus of 1999 (Loeb *et al.,* 2018).

*4.5 Atlantic Tropical Cyclones*

This example illustrates the application of Hurst rescaling to count data with a dataset for which known observational difficulties exist. Annual numbers of named storms (*i.e.*, tropical storms and hurricanes) for the North Atlantic Basin were obtained from the NHC HURDAT2

archive (*https://www.nhc.noaa.gov/data/*, downloaded on May 7, 2021) from the 1851 to 2020 tropical cyclone seasons (Landsea and Franklin, 2013). These data were based on the maximum Saffir-Simpson category assigned to the storm during post-storm analysis. Results also were examined for hurricanes and major hurricanes with similar conclusions (not shown). For more information on how these data were compiled, see Landsea *et al.* (2004) and Landsea and Franklin (2013).

The annual number of named storms (Figure 7a) shows considerable variability over the entire period of record with little trend from 1851 to 1930, a slight increase through the 1960s, a slight decrease in the 1970s and 1980s, and a decided increase after about 1995. However, the normalized rescaled running sum (Figure 7b) shows two marked changes occurring in 1930 and again in 1995. An analysis of just the tropical cyclone numbers (deleting events that reached only tropical storm status) suggests additional small discontinuities in about 1893 and 1947, although these discontinuities do not appear significant when only major hurricanes (Category 3 or higher on the Saffir-Simpson scale) are considered (not shown). However, the analysis of major hurricanes does suggest a discontinuity around 1910. Note that while Chylek and Lesins (2008) suggest a sixty-year cycle for hurricane numbers exists and that two full cycles are present in the data (*i.e.*, 1860-1920 and 1920-1980), this sixty-year cycle does not present a discontinuity in the record, nor does it adversely affect the analysis of the normalized rescaled running sum.

The marked change in the time series in 1930 corresponds to a change from a once daily estimate of tropical cyclone position and intensity (12Z) to a six-hourly set of measurements, which could create issues associated with rapid storm intensification or decay (Landsea *et al.,* 2004). In addition, the inclusion of daily surface synoptic maps for the Northern Hemisphere in

the late 1920s and the development of wind tunnels to allow proper calibration of anemometers in the 1920s also may contribute to the discontinuity near 1930 (Landsea *et al.,* 2004).

Another large discontinuity is suggested on or about 1995. Landsea and Franklin (2013) note that for tropical cyclone reanalysis, best track data transitioned from four times per day to the nearest minute (in time). They also note that additional records, which do not align with synoptic measurement times (such as for tropical cyclone landfall or peak intensity) were incorporated into the reanalysis for data prior to 1945 and after 1991 (Landsea and Franklin, 2013). This and the inclusion of aircraft reconnaissance data in the mid-1940s (Landsea *et al.,* 2004) also may explain the small discontinuity present near 1947 in the hurricane-only data.

The apparent discontinuities on or about 1893 in the hurricane numbers and near 1910 in the major hurricane numbers may be an artifact of the incorporation of work by Partagas and Diaz (1996). See also Landsea *et al.* (2004:180) where incorporation of their research "led to the creation of completely new tropical cyclone tracks and intensities for the years 1851 to 1885 and the alteration of existing track and intensity data for the period of 1886 to 1910." Similarly, reanalysis efforts found and adjusted errors in the 1886 to 1910 data (Landsea *et al.,* 2004).

*4.6 Central England Air Temperatures*

The Hadley Centre air temperature data (monthly averages) for central England (a triangle from London, to Bristol, to Lancashire) were obtained from the United Kingdom Meteorological Office archive (*https://www.metoffice.gov.uk/hadobs/hadcet/*, downloaded on August 14, 2021, CETv1) from 1659 to 2020 (Parker *et al.,* 1992, Parker and Horton, 2005). These data were created by updating and extending Manley's (1974) monthly temperature time series for central England. Station adjustments were made to representative central England air temperatures by evaluating

the urban heat island effect (through comparison with neighboring rural stations). The Hadley Centre Central England Temperature (HadCET) dataset purports to be the longest instrumental record of air temperature available anywhere.

Central England air temperature (Figure 8a) exhibits much temporal variability with a significant decrease in the 17th century, a relatively constant temperature through the mid-20th century (with some trends on multi-decadal scales), and subsequent warming from the latter half of the 20th century into the 21st century. A significant single-year drop in air temperature occurs in 1740 (~ -2.4C°) and 1879 (~ -1.5C°). Concomitant with these trends, the normalized rescaled running sum (Figure 8b) divides the time series into four periods – the 17th century through the first quarter of the 18th century, from the early 1700s until the late 1800s, most of the 20th century (until about 1990), and then the last thirty-year period (Figure 8b).

The first apparent discontinuity is coincident with the quote by Manley (1974:393), "for the first six decades to 1720 the figures are printed in italics as an indication that they must be considered less reliable, based as they are on extrapolation from the results of readings of highly imperfect instruments in uncertain exposures at a considerable distance…or on estimates based on interpretations of daily observations of wind and weather." Data prior to 1671 were rounded to the nearest whole C° owing to imprecise instrumental readings while some values from 1707 to 1722 were derived "from analysis of snowfall frequency from a careful analysis of observed snowfall frequency and from the overlapping series of monthly means representative of Utrecht…coupled with wind directions" (Manley, 1974:393). Although the Hadley Centre database includes estimations at a higher observational resolution (*i.e.,* to the nearest 0.1C°), Manley's (1974) observations indicate that reliability of data prior to 1722 is much less than the remainder of the time series.

The second apparent discontinuity occurs in the late 19th century. Parker *et al.* (1992) notes that a single station (*i.e.,* one data point) comprises much of the composite record from 1772 to 1876. Moreover, Parker and Horton (2005) indicate that systematic adjustments (±0.2C°) were applied to data from 1878 to 1921 (but not before 1878) and although the maximum and minimum air temperatures usually had adjustments of different signs, the mean air temperature would have been affected to some extent. As for the final discontinuity, Parker *et al.* (1992) observe that urban warming was significant from about 1974 onwards while Parker and Horton (2005) apply a systematic bias adjustment (±0.1C°) to data from 1980 onwards.

**5 Discussion**

Hurst rescaling has been known for more than two decades (Outcalt *et al.,* 1997) but it still represents a robust and obvious approach to examining a time series for both natural breakpoints and data biases. Inflection points (*i.e.*, significant changes in the slope of the integral trace) in the integral trace delineate transitions from one climate regime to another or a significant change in the manner that data are collected (*e.g.*, changes in data measurement, its location of measurement, and/or the time of measurement). Statistically, a significant inflection point identifies when this regime change occurs. Moreover, sign of the slope of the integral trace indicates the temporal persistence of the time series (*i.e*., a positive slope implies a persistence of observations above the mean while a negative slope indicates persistence below the mean) while the magnitude of the slope represents the temporal clustering of similar extremes (Outcalt *et al.,* 1997).

The examples shown here demonstrate that Hurst rescaling can be applied across a wide variety of geophysical variables, including climatologically and hydrologically oriented time series. Outcalt *et al.* (1997) raises the issue that Hurst rescaling requires regime lengths of relatively long runs; however, this is a standard statistical argument. Short runs are difficult to

identify as a true, short-lived regime rather than a small random fluctuation of a larger regime. Therefore, Hurst rescaling should be used to identify significant changes and an attempt should not be made to analyze every small fluctuation in the integral trace. Thus, Hurst rescaling provides a unique and viable approach to detect changes in atmospheric time series, even in cases where almost no temporal autocorrelation exists.

Many other methods to identify discontinuities in a time series have been posited over the years (see Weatherhead *et al.,* 1998; Reeves *et al.,* 2007; Mudelsee, 2019; Muthuramu and Maheswari, 2019). Such methods usually seek to identify structural breaks or changepoints using a variety of different approaches including autoregressive and autoregressive-moving averages (Karl *et al.,* 2000; Seidel and Lanzante, 2004; Davis *et al.,* 2006), regression-based coefficients and methods (Jouini and Boutahar, 2005; Dixon and Moore, 2011; Lyubchich *et al.,* 2013; Aue and Horváth, 2013; Guo *et al.,* 2018; Elder and Fong, 2019; Tharu and Dhakal, 2020), t- or F-tests with hypothesis testing (Lund *et al.,* 2007; Rienzner and Gandolfi, 2011; Gallagher *et al.,* 2013), higher-order moments of the distribution (Hilas *et al.,* 2013; Xie *et al.,* 2019) and cumulative sums (Shao and Zhang, 2010), Bayesian methods (Ruggieri, 2013; Chen *et al.,* 2017; Yu and Ruggieri, 2019), bootstrap approaches (Bickel and Ren, 2001; Noguchi *et al.,* 2011; Lyubchich *et al.,* 2013), classification analysis (Anders *et al.,* 2013), manifold learning models (Xie *et al.,* 2013), functional data analysis (Alaya *et al.,* 2020), an informational approach (Beaulieu *et al.,* 2012), and nonparametric methods (Lanzante, 1996; Douglas *et al.,* 2000; Burn and Elnur, 2002; Xiong and Guo, 2004; McKitrick and Vogelsang, 2014; Xie *et al.,* 2014; Basarir *et al.,* 2017; Guo *et al.,* 2018; Hajani and Rahman, 2018; Zhou *et al.,* 2019; Bagniewski *et al.,* 2021). Most of these techniques work directly with the series in the time domain, usually searching for changes in parameters of the distribution or trend or shifts in the moments of the time series (*e.g.*, mean, kurtosis) across a

change point, although other researchers have explored the use of Hurst statistics to changepoint analyses (Outcalt *et al.,* 1997; Tan and Gan, 2017). The advantage of the integral trace is that rather than examining the time domain – where trends, patterns, and discontinuities may be obscured or difficult to detect – the integral trace can be considered as a mixed ARMA process (Wallis and O'Connell, 1973; Boes and Salas, 1978).

It has also been suggested that smoothing of the time series (*i.e.,* low-pass filtering) can enhance detection of change points and discontinuities (*e.g.*, You *et al.,* 2018). We strongly recommend against this as smoothing tends to involve subjective decisions that can adversely affect the outcome (Howarth and Rogers, 1992) but more importantly, discontinuities in the time series are often obscured or masked and temporal fidelity can be undermined (Esper *et al.,* 2005).

## ACKNOWLEDGMENTS

We are indebted to comments from Any Iliopoulou and Demetris Koutsoyiannis, who contributed extensively to the discussion on Hurst statistics, on an earlier draft of our manuscript. We also are indebted to two anonymous reviewers for their thorough comments on our manuscript. Neither of the authors received any funding for this research.

## CONFLICT OF INTEREST

The authors declare no potential conflict of interests.

## ORCHID

David R. Legates https://orcid.org/0000-0003-4323-4416

**Figure Captions**

**Figure 1:** Time series of Northern Hemisphere air temperature from Moberg *et al.* (2005) (top) and a simulated "climate" having the same variance as the Moberg *et al.* time series but generated from the average of twelve spins of a roulette wheel (bottom). Figure taken from Koutsoyiannis and Cohn (2008).

**Figure 2:** Raw observations from a hypothetical distribution (a) and its normalized rescaled running sum as a function of time (b).

**Figure 3:** Monthly Pacific Decadal Oscillation (PDO from Nate Mantua) (a) and its normalized rescaled running sum as a function of time (b).

**Figure 4:** Thaw depths (in cm) for the four locations in northern Alaska (a) and their normalized rescaled running sum as a function of time (b).

**Figure 5:** Maximum Northern Hemisphere snow cover extent (in $km^2$) (a) and its normalized rescaled running sum as a function of time (b).

**Figure 6:** Maximum river flow (in $m^3 s^{-1}$) at Lees Ferry, Colorado (a) and its normalized rescaled running sum as a function of time for the entire period of record (b).

**Figure 7:** Total number of named storms (per year) in the North Atlantic basin (a) and its normalized rescaled running sum as a function of time (b).

**Figure 8:** Central England air temperature (C°) (a) and its normalized rescaled running sum as a function of time (b).

**Table Captions**

**Table 1:** Simple example of a dataset with discontinuities. The observations ($X_t$) are taken from a Gaussian normal distribution that are $N(20,2)$ for $t = 1,15$, $N(22,2)$ for $t = 16,34$, and $N(22,4)$ for $t = 35,50$. Data are rounded to two decimal places.

**References**

Alaya, M.A.B., Ternynck, C., Dabo-Niang, S., Chebana, F., and Ouarda, T.B.M.J. 2020. Change point detection of flood events using a functional data framework. *Adv. Water Resour.* **137**, 103522. doi: 10.1016/j.advwatres.2020.103522

Anders, N.S., Seijmonsbergen, A.C., and Bouten, W. 2013. Geomorphological change detection using object-based feature extraction from multi-temporal LiDAR data. *IEEE Geosci. Remote Sens. Lett.* **10**(6), 1587-1591. doi: 10.1109/LGRS.2013.2262317

Andrade, J.M., and Estévez-Pérez, M.G. 2014. Statistical comparison of the slopes of two regression lines: A tutorial. *Anal. Chim. Acta* **838**, 1-12. doi: 0.1016/j.aca.2014.04.057

Aue, A., and Horváth, L. 2013. Structural breaks in time series. *J. Time Ser. Anal.* **34**, 1-16. doi: 10.1111/j.1467-9892.2012.00819.x

Bagniewski, W., Ghil, M., and Rousseau, D.D. 2021. Automatic detection of abrupt transitions in paleoclimate records. *Chaos* **31**(113129). doi: 10.1063/5.0062543

Barton, D.E., and David, F.N. 1957. Multiple runs. *Biometrika* **44**(1-2), 168-178. doi: 10.1093/biomet/44.1-2.168

Basarir, A., Arman, H., Hussein, S., Murad, A., Aldahan, A., and Al-Abri, M.A. 2017. Trend detection in climate change indicators using non-parametric statistics: A case study of Abu Dhabi, United Arab Emirates. *Acta Phys. Pol. A* **132**, 655-657. doi: 10.12693/APhysPolA.132.655

Beaulieu, C., Chen, J., and Sarmiento, J.L. 2012. Change-point analysis as a tool to detect abrupt climate variations. *Phil. Trans. R. Soc. A* **370**, 1228-1249. doi: 10.1098/rsta.2011.0383

Bickel, P.J., and Ren, J.-J. 2001. *The bootstrap in hypothesis testing.* In *State of the Art in Probability and Statistics*. M. de Gunst, C. Klaassen, and A. van der Vaart, eds., Institute of Mathematical Physics, 91-112. doi: 10.1214/lnms/1215090064

Boes, D.C., and Salas, J.D. 1978. Nonstationarity of the mean and the Hurst phenomenon. *Water Resour. Res.* **14**(1), 135-143. doi: 10.1029/WR014i001p00135

Bond, N.A., Overland, J.E., Spillane, M., and Stabeno, P.J. 2003. Recent shifts in the state of the North Pacific. *Geophys. Res. Lett.* **30**(23), 2183. doi: 10.1029/2003GL018597

Bond, N.A., Cronin, M.F., Freeland, H., and Mantua, N. 2015. Causes and impacts of the 2014 warm anomaly in the NE Pacific. *Geophys. Res. Lett.* **42**(9), 3414-3420. doi: 10.1002/2015GL063306

Briggs, W.M. 2017. The substitute for *p*-values. *J. Am. Stat. Assoc.* **112**(519), 897-898. doi: 10.1080/01621459.2017.1311264

Briggs, W.M. 2019. Everything wrong with *p*-values under one roof. In *Beyond Traditional Probabilistic Methods in Economics.* V. Kreinovich *et al.*, eds., Springer International Publishing, Studies in Computational Intelligence 809, 22-44.

Briggs, W.M., Nguyen, H.T., and Trafimow, D. 2019. The replacement for hypothesis testing. In *Structural Changes and the Econometric Modeling*. V. Kreinovich and S. Sriboonchitta, eds., Springer International Publishing, Studies in Computational Intelligence 808, 3-17.

Budyko, M.I. 1948. *Evaporation Under Natural Conditions.* Gedrometeoizdat, St. Petersburg, Russia, 29pp.

Burn, D.H., and Elnur, M.A.H. 2002. Detection of hydrologic trends and variability. *J. Hydrol.* **255**, 107-122. doi: 10.1016/S0022-1694(01)00514-5

Ceballos, R.F., and Largo, F.F. 2017. On the estimation of the Hurst exponent using adjusted rescaled range analysis, detrended fluctuation analysis and variance time plot: A case of exponential distribution. *Imp. J. Interdiscip. Res.* **3**(8), 424-434.

Cech, T.V. 2009. *Principles of Water Resources: History, Development, Management, and Policy, 4th Edition*. John M. Wiley & Sons, Hoboken NJ, 509pp.

Chen, S., Li, Y., Kim, J., and Kim, S.W. 2017. Bayesian change point analysis for extreme daily precipitation. *Int. J. Climatol.* **37**, 3123-3137. doi: 10.1002/joc.4904

Chow, G.C. 1960. Tests of equality between sets of coefficients in two linear regressions. *Econometrica* **28**(3), 591-605. doi: 10.2307/1910133

Chylek, P., and Lesins, G. 2008. Multidecadal variability of Atlantic hurricane activity: 1851-2007. *J. Geophy. Res.* **113**, D22106. doi: 10.1029/2008JD010036

Clarke, R.T. 2010. On the (mis)use of statistical methods in hydro-climatological research. *Hydrol. Sci. J.* **55**(2), 139-144. doi: 10.1080/02626661003616819

Cohn, T.A., and Lins, H.F. 2005. Nature's style: Naturally trendy. *Geophys. Res. Lett.* **32**, L23402. doi: 10.1029/2005GL024476

Davis, R.., Lee, T.C.M., and Rodriguez-Yam, G.A. 2006. Structural break estimation for nonstationary time series models. *J. Am. Stat. Assoc.* **101**(473), 223-239. doi: 10.1198/016214505000000745

Dias, N.L., Crivellaro, B.L., and M. Chamecki. 2018. The Hurst phenomenon in error estimates related to atmospheric turbulence. *Bound.-Layer Meteorol.* **168**, 387-416. doi: 10.1007/s10546-018-0353-7

Dimitriadis, P., and D. Koutsoyiannis, 2015. Climacogram versus autocovariance and power spectrum in stochastic modelling for Markovian and Hurst–Kolmogorov processes. *Stoch. Environ. Res.* Risk Assess. **29**(6), 1649-1669. doi: 10.1007/s00477-015-1023-7

Ding, H., Greatbatch, R.J., Latif, M., Park, W., and Gerdes, R. 2013. Hindcast of the 1976/77 and 1998/99 climate shifts in the Pacific. *J. Clim.* **26**(19), 7650-7661. doi: 10.1175/JCLI-D-12-00626.1

Dixon, R.W., and Moore, T.W. 2011. Trend detection in Texas temperature and precipitation. *Southwest. Geogr.* **15**, 80-103.

Douglas, E.M., Vogel, R.M., and Kroll, C.N. 2000. Trends in floods and low flows in the United States: Impact of spatial correlation. *J. Hydrol.* **240**(1-2), 90-105. doi: 10.1016/S0022-1694(00)00336-X

Elder, A., and Fong, Y. 2019. Estimation and inference for upper hinge regression models. *Environ. Ecol. Stat.* **26**, 287-302. doi: 10.1007/s10651-019-00428-1

Esper, J., Frank, D.C., Wilson, R.J.S., and Briffa, K.R. 2005. Effect of scaling and regression on reconstructed temperature amplitude for the past millennium. *Geophys. Res. Lett.* **32**(L07711). doi: 10.1029/2004GL021236

Estilow, T.W., Young, A.H., and Robinson, D.A. 2015. A long-term Northern Hemisphere snow cover extent data record for climate studies and monitoring. *Earth Syst. Sci. Data* **7**, 137-142, doi: 10.5194/essd-7-137-2015

Fagerland, M.W. 2012. t-tests, non-parametric tests, and large studies – a paradox of statistical practice? *BMC Med. Res. Methodol.* **12**(78), 7pp. doi: 10.1186/1471-2288-12-78

Fischer, H.B. (1973). A possible explanation for Nordin, McQuivey, and Majia's observation of the Hurst phenomenon in turbulence. *Water Resour. Res.* **9**(2), 492-493. doi: 10.1029/WR009i002p00492

Gallagher, C., Lund, R., and Robbins, M. 2013. Changepoint detection in climate time series with long-term trends. *J. Clim.* **26**(14), 4994-5006. doi: 10.1175/JCLI-D-12-00704.1

Gan, T.Y., Barry, R.G., Gizaw, M., Gobena, A., and Balaji, R. 2013. Changes in North American snowpacks for 1979-2007 detected from the snow water equivalent data of SMMR and SSM/I passive microwave and related climatic factors. *J. Geophys. Res. Atmos.* **118**, 7682-7697, doi: 10.1002/jgrd.50507

Gedalof, Z., and Smith D.J. 2001. Interdecadal climate variability and regime-scale shifts in Pacific North America. *Geophys. Res. Lett.* **28**(8), 1515-1518. doi: 10.1029/2000GL011779

Giese, B.S., Urizar, S.C., and Fuckar, N.S. 2001. Southern Hemisphere origins of the 1976 climate shift. *Geophys. Res. Lett.* **29**(2), 1014. doi: 10.1029/2001GL013268

Guo, L.-P., Yu, Q., Gao, P., Nie, X.-F., Liao, K.-T., Chen, X.-L., Hu, J.-M., and Mu, X.-M. 2018. Trend and change-point analysis of streamflow and sediment discharge of the Gongshui River in China during the last 60 years. *Water* **10**(1273), 19pp. doi: 10.3390/w10091273

Hajani, E., and Rahman, A. 2018. Characterizing changes in rainfall: A case study for New South Wales, Australia. *Int. J. Climatol.* **38**, 1452-1462. doi: 10.1002/joc.5258

Halsey, L.G. 2019. The reign of the *p*-value is over: What alternative analyses could we employ to fill the power vacuum? *Biol. Lett.* **15**(20190174), 8pp. doi: 10.1098/rsbl.2019.0174

Hamed, K.H. 2007. Improved finite-sample Hurst exponent estimates using rescaled range analysis. *Water Resour. Res.* **43**(4), W04413. doi: 10.1029/2006WR005111

Hartmann, B., and Wendler, G. 2005. The significance of the 1976 Pacific Climate Shift in the climatology of Alaska. *J. Clim.* **18**(22), 4824-4839. doi: 10.1175/JCLI3532.1

Hartmann, D.L. 2015. Pacific sea surface temperature and the winter of 2014. *Geophys. Res. Lett.* **42**(6), 1894-1902. doi: 10.1002/2015GL063083

Hidalgo, H.G., and Dracup, J.A. 2003. ENSO and PDO effects on hydroclimatic variations of the upper Colorado River. *J. Hydrometeorol.* **4**(1), 5-23. doi: 10.1175/1525-7541(2003)004<0005:EAPEOH>2.0.CO;2

Hilas, C.S., Rekanos, I.T., and Mastorocostas, P.A. 2013. Change point detection in time series using higher-order statistics: A heuristic approach. *Math. Probl. Eng.* **2013**(317613), 10 pp. doi: 10.1155/2013/317613

Hinkel, K.M., and Outcalt, S.I. 1995. Detection of heat-mass transfer regime transitions in the active layer using fractal geometric parameters. *Cold Reg. Sci. Technol.* **23**, 293-304. doi: 10.1016/0165-232X(95)00003-T

Hjellvik, V., and Tjøstheim, D. 1995. Nonparametric tests of linearity for time series. *Biometrika* **82**(2), 351-368. doi: 10.1093/biomet/82.2.351

Howarth, D.A., and Rogers, J.C. 1992. Problems associated with smoothing and filtering of geophysical time-series data. *Phys. Geogr.* **13**(1), 81-99. doi: 10.1080/02723646.1992.10642446

Hurrell, J.W., and van Loon, H. 1994. A modulation of the atmospheric annual cycle in the Southern Hemisphere. *Tellus* **46A**(3), 325-338. doi: 10.1034/j.1600-0870.1994.t01-1-00007.x

Hurst, H.E. 1951. Long-term storage capacity of reservoirs. *T. Am. Soc. Civ. Eng.* **116**, 770-799.

Hurst, H.E. 1956. The problem of long-term storage in reservoirs. *Hydrol. Sci. J.* **1**(3), 13-27. doi: 10.1080/02626665609493644

Istanbulluoglu, E., Wang, T., Wright, O.M., and Lenters, J.D. 2012. Interpretation of hydrologic trends from a water balance perspective: The role of groundwater storage in the Budyko hypothesis. *Water Resour. Res.* **48**(W00H16). doi: 10.1029/2010WR010100

Johnstone, J.A., and Mantua, N.J. 2014. Atmospheric controls on northeast Pacific temperature variability and change, 1900-2012. *Proc. Natl. Acad. Sci. U.S.A.* **111**(40), 14360-14365. doi: 10.1073/pnas.1318371111

Jouini, J., and Boutahar, M. 2005. Evidence on structural changes in U.S. time series. *Econ. Model.* **22**, 391-422. doi: 10.1016/j.econmod.2004.06.003

Karl, T.R., Knight, R.W., and Baker, B. 2000. The record breaking global temperatures of 1997 and 1998: Evidence for an increase in the rate of global warming? *Geophys. Res. Lett.* **27**, 719-722. doi: 10.1029/1999GL010877

Kenkel, N.C. 1995. Environmental persistence and the structure/composition of northern prairie marshes. *UFS (Delta Marsh) Annual Report* **30**, 93-98.

Khaliq, M.N., and Gachon, P. 2010. Pacific Decadal Oscillation climate variability and temporal pattern of winter flows in Northwestern North America. *J. Hydrometeorol.* **11**(4), 917-933. doi: 10.1175/2010JHM1254.1

Khapalova, E.A., Jandhyala, V.K., Fotopoulos, S.B., and Overland, J.E. 2018. Assessing change-points in surface air temperature over Alaska. *Front. Environ. Sci.* **6**(121). doi: 10.3389/fenvs.2018.00121

Klemeš, V. 1974. The Hurst phenomenon: A puzzle? *Water Resour. Res.* **10**(4), 675-688. doi: 10.1029/WR010i004p00675

Klemeš, V. 1986. Dilettantism in hydrology: Transition or destiny. *Water Resour. Res.* **22**(9), 177S-188S. doi: 10.1029/WR022i09Sp0177S

Koutsoyiannis, D., 2002. The Hurst phenomenon and fractional Gaussian noise made easy. *Hydrol. Sci. J.* **47**(4), 573-595. doi: 10.1080/02626660209492961

Koutsoyiannis, D., 2005a. Uncertainty, entropy, scaling and hydrological stochastics, 1, Marginal distributional properties of hydrological processes and state scaling. *Hydrol. Sci. J.* **50**(3), 381-404. doi: 10.1623/hysj.50.3.381.65031

Koutsoyiannis, D., 2005b. Uncertainty, entropy, scaling and hydrological stochastics, 2, Time dependence of hydrological processes and time scaling. *Hydrol. Sci. J.* **50**(3), 405-426. doi: 10.1623/hysj.50.3.405.65028

Koutsoyiannis, D. 2013. Hydrology and change. *Hydrol. Sci. J.* **58**(6), 1177-1197. doi: 10.1080/02626667.2013.804626

Koutsoyiannis, D., and Cohn, T.A. 2008. *The Hurst phenomenon and climate*. European Geosciences Union General Assembly, Vienna, Austria, European Geosciences Union. doi: 10.13140/RG.2.2.13303.01447

Koutsoyiannis, D., and Montanari, A. 2015. Negligent killing of scientific concepts: The stationarity case. *Hydrol. Sci. J.* **60**(7-8), 1174-1183. doi: 10.1080/02626667.2014.959959

Koutsoyiannis, D., Efstratiadis, A., Mamassis, N., and Christofides, A. 2008. On the credibility of climate predictions. *Hydrol. Sci. J.* **53**(4), 671-684. doi: 10.1623/hysj.53.4.671

Koutsoyiannis, D., Dimitriadis, P, Lombardo, F., and Stevens, S. 2018. From fractals to stochastics: Seeking theoretical consistency in analysis of geophysical data. In *Advances in Nonlinear Geosciences*. A.A. Tsonis, ed., Springer International Publishing**,** 237-278.

Kubota, H., and Chan, J.C.L. 2009. Interdecadal variability of tropical cyclone landfall in the Philippines from 1902 to 2005. *Geophys. Res. Lett.* **36**, L12802. doi: 10.1029/2009GL038108

Landsea, C.W., and Franklin, J.L. 2013. Atlantic hurricane database uncertainty and presentation of a new database format. *Mon. Wea. Rev.* **141**(10), 3576-3592. doi:10.1175/MWR-D-12-00254.1

Landsea, C.W., Anderson, C., Charles, N., Clark, G., Dunion, J.P., Fernandez-Partagas, J., Hungerford, P., Neumann, C.J., and Zimmer, M. 2004. The Atlantic hurricane database re-analysis project: Documentation for 1851-1910 alterations and additions to the HURDAT database. In *Hurricanes and Typhoons: Past, Present, and Future*. R.J. Nurnane and K.B. Liu, eds., Columbia University Press, 178-219.

Lanzante, J.R. 1996. Resistant, robust and non-parametric techniques for the analysis of climate data: Theory and examples, including applications to historical radiosonde station data. *Int. J. Climatol.* **16**, 1197-1226. doi: 10.1002/(SICI)1097-0088(199611)16:11<1197::AID-JOC89>3.0.CO;2-L

Litzow, M.A., Hunsicker, M.E., Bond, N.A., *et al.* 2020. The changing physical and ecological meanings of North Pacific Ocean climate indices. *Proc. Natl. Acad. Sci. U.S.A.* **117**(14), 7665-7671. doi: 10.1073/pnas.1921266117

Loeb, N.G., Thorsen, T.J., Norris, J.R., Wang, H., and Su, W. 2018. Changes in Earth's energy budget during and after the "pause" in global warming: An observational perspective. *Climate* **6**(62), 18pp. doi: 10.3390/cli6030062

Lund, R., Wang, X.L., Lu, Q.Q., Reeves, J., Gallagher, C., and Feng, Y. 2007. Changepoint detection in periodic and autocorrelated time series. *J. Clim.* **20**(20), 5178-5190. doi: 10.1175/JCLI4291.1

Lupo, A.R., Latham, T.K., Magill, T.H., Clark, J.V., Melick, C.J., and Market, P.S. 2008. The interannual variability of hurricane activity in the Atlantic and East Pacific regions. *Natl. Weather Dig.* **32**(1), 11-33.

Lyubchich, V., Gel, Y.R., and El-Shaarawi, A.H. 2013. On detecting non-monotonic trends in environmental time series: A fusion of local regression and bootstrap. *Environmetrics* **24**, 209-226. doi: 10.1002/env.2212

Ma, L., and Yin, Z. 2017. Possible solar modulation of the Pacific Decadal Oscillation. *Sol. Syst. Res.* **51**(5), 417-421. doi: 10.1134/S0038094617050069

Mandelbrot, B.B. 1982. *The Fractal Geometry of Nature*. W.H. Freeman & Co., New York. 468pp. ISBN-13: 978-0716711865.

Mantua, N.J., Hare, S.R., Zhang, Y., Wallace, J.M., and Francis, R.C. 1997. A Pacific interdecadal climate oscillation with impacts on salmon production. *Bull. Amer. Meteor. Soc.* **78**(6), 1069-1079. doi: 10.1175/1520-0477(1997)078<1069:APICOW>2.0.CO;2

Manley, G. 1974. Central England temperatures: Monthly means 1659 to 1973. *Q.J.R. Meteorol. Soc.*, **100**(425), 389-405. doi: 10.1002/qj.49710042511

Mauget, S.A. 2015. Optimal ranking regime analysis of treeflow dendrohydrological reconstructions. *Clim. Past* **11**, 1107-1125. doi: 10.5194/cp-11-1107-2015

McCabe, G.J. Jr., Palecki, M.A., and Betancourt, J.L. 2004. Pacific and Atlantic Ocean influences on multidecadal drought frequency in the United States. *Proc. Natl. Acad. Sci. U.S.A.* **101**(12), 4136-4141. doi: 10.1073/pnas.0306738101

McKitrick, R.R., and Vogelsang, T.J. 2014. HAC robust trend comparisons among climate series with possible level shifts. *Environmetrics* **25**, 528-547. doi: 10.1002/env.2294

McShane, B.B. and Gal, D. 2017. Statistical significance and the dichotomization of evidence. *J. Am. Stat. Assoc.* **112**(519), 885-908. doi: 10.1080/01621459.2017.1289846

Meehl, G.A., Hu, A., and Santer, B.D. 2009. The mid-1970s climate shift in the Pacific and the relative roles of forced versus inherent decadal variability. *J. Climatol.* **22**(3), 780-792. doi: 10.1175/2008JCLI2552.1

Meko, D.M., Woodhouse, C.A., Baisan, C.A., Knight, T., Lukas, J.J., Hughes, M.K., and Salzer, M.W. 2007. Medieval drought in the upper Colorado River Basin. *Geophys. Res. Lett.* **34**(L10705). doi: 10.1029/2007GL029988

Mesa, O.J., and Poveda, G. 1993. The Hurst effect: The scale of fluctuation approach. *Water Resour. Res.* **29**(12), 3995-4002. doi: 10.1029/93WR01686

Miller, A.J., Cayan, D.R., Barnett, T.P., Graham, N.E., and Oberhuber, J.M. 1994. The 1976-77 climate shift of the Pacific Ocean. *Oceanography* **7**(1), 21-26. doi: 10.5670/oceanog.1994.11

Moberg, A., Sonechkin, D.M., Holmgren, K., Datsenko, N.M., and Karlen, W. 2005. Highly variable Northern Hemisphere temperatures reconstructed from low- and high-resolution proxy data. *Nature* **433,** 613-617. doi: 10.1038/nature03265

Mudelsee, M. 2019. Trend analysis of climate time series: A review of methods. *Earth-Sci. Rev.* **190**, 310-322. doi: 10.1016/j.earscirev.2018.12.005

Muthuramu, P., and Maheswari, T.U. 2019. Tests for structural breaks in time series analysis: A review of recent development. *Shanlax Int. J. Econom.* **7**, 66-79. doi: 10.34293/economics.v7i4.628

Nakagawa, S., and Cuthill, I.C. 2007. Effect size, confidence interval and statistical significance: A practical guide for biologists. *Biol. Res.* **83**, 591-605. doi: 10.1111/j.1469-185X.2007.00027.x

Nelson, F.E., Outcalt, S.I., Brown, J., Shikomanov, N.I., and Hinkel, K.M. 1998. Spatial and temporal attributes of the active-layer thickness record, Barrow, Alaska, U.S.A. *7th International Conference on Permafrost,* 797-802.

Niu, K., Hu, Q., Wang, Y., Yang, H., Liang, C., *et al.* 2021. Analysis on the variation of hydro-meteorological variables in the Yongding River Mountain Area driven by multiple factors. *Remote Sens.* **13**(3199). doi: 10.3390/rs13163199

Noguchi, K., Gel, Y.R., and Duguay, C.R. 2011. Bootstrap-based tests for trends in hydrological time series, with application to ice phenology data. *J. Hydrol.* **410**, 150-161. doi: 10.1016/j.jhydrol.2011.09.008

Nordin, C.F., McQuivey, R.S., and Mejia, J.M. 1972. Hurst phenomenon in turbulence. *Water Resour. Res.* **8**(6), 1480-1486. doi: 10.1029/WR008i006p01480

O'Connell, P.E., Koutsoyiannis, D., Lins, H.F., Markonis, Y., Montanari, A., and Cohn, T.A. 2016. The scientific legacy of Harold Edwin Hurst (1880–1978). *Hydrol. Sci. J.* **61**(9), 1571-1590. doi: 10.1080/02626667.2015.1125998

Osterkamp, T.E., Zhang, T., and Romanovsky, V.E. 1994. Evidence for a cyclic variation of permafrost temperatures in Northern Alaska. *Permafr. Periglac. Process.* **5**, 137-144. doi: 10.1002/ppp.3430050303

Outcalt, S.I. 1972. A reconnaissance experiment in mapping and modeling the effect of land use on urban thermal regimes. *J. Appl. Meteorol.* **11**(12), 1369-1373. doi: 10.1175/1520-0450(1972)011<1369:AREIMA>2.0.CO;2

Outcalt, S.I. 2015. The treeflow record from Lees Ferry, Arizona: 762-2005 A.D. Unpublished manuscript.

Outcalt, S.I. 2018. Thaw depth in Northern Alaska: The conformation of major global climate transitions in the mid 1970's and early 21st century. Unpublished manuscript.

Outcalt, S.I., and Melton, M.A. 1992. Geomorphic application of the Hausdorff-Besicovich dimension. *Earth Surf. Process. Landf.* **17**, 775-787. doi: 10.1002/esp.3290170805

Outcalt, S.I., Hinkel, K.M., Meyer, E., and Brazel, A.J. 1997. Application of Hurst rescaling to geophysical serial data. *Geogr. Anal.* **29**(1), 72-87. doi: 10.1111/j.1538-4632.1997.tb00947.x

Overpeck, J., Hughen, K., Hardy, D., Bradley, R., Case, R., Douglas, M., Finney, B., Gajewski, K., Jacoby, G., Jennings, A., Lamoureux, S., Lasca, A., MacDonald, G., Moore, J., Retelle, M., Smith, S., Wolfe, A., and Zielinski, G. 1997. Arctic environmental change of the last four centuries. *Science* **278**, 1251-1256. doi: 10.1126/science.278.5341.1251

Parker, D.E., and Horton, B. 2005. Uncertainties in central England temperature 1878-2003 and some improvements to the maximum and minimum series. *Int. J. Climatol.* **25**, 1173-1188. doi: 10.1002/joc.1190

Parker, D.E., Legg, T.P., and Folland, C.K. 1992. A new daily central England temperature series, 1772-1991. *Int. J. Climatol.* **12**(4), 317-342. doi: 10.1002/joc.3370120402

Partagas, J.F., and Diaz, H.F. 1996. Atlantic hurricanes in the second half of the nineteenth century. *Bull. Amer. Meteor. Soc.,* **77**(12), 2877-2906. doi: 10.1175/1520-0477(1996)077<2899:AHITSH>2.0.CO;2

Pease, R.W., Lewis, J.E., and Outcalt, S.I. 1976. Urban terrain climatology and remote sensing. *Ann. Assoc. Am. Geogr.* **66**(4), 557-569. doi: 10.1111/j.1467-8306.1976.tb01110.x

Polovina, J., Mitchum, G.T., Graham, N.E., Craig, M.P., DeMartini, E.E., and Flint, E.N. 1994. Physical and biological consequences of a climatic event in the Central North Pacific. *Fisheries Oceanogr.* **3**, 15-21. doi: 10.1111/j.1365-2419.1994.tb00044.x

Potter, K.W. 1976. Evidence for nonstationarity as a physical explanation of the Hurst phenomenon. *Water Resour. Res.* **12**(5), 1047-1052. doi: 10.1029/WR012i005p01047

Potter, K.W. 1979. Annual precipitation in the Northeast United States: Long memory, short memory, or no memory? *Water Resour. Res.* **15**(2), 340-346. doi: 10.1029/WR015i002p00340

Reeves, J., Chen, J., Wang, X.L., Lund, R., and Lu, Q.Q. 2007. A review and comparison of changepoint detection techniques for climate data. *J. Appl. Meteorol. Clim.* **46**(6), 900-915. doi: 10.1175/JAM2493.1

Rice, J.L., Woodhouse, C.A., and Lukas, J.J. 2009. Science and decision making: Water management and tree-ring data in the western United States. *J. Am. Water Resour. Assoc.* **45**(5), 1248-1259. doi: 10.1111/j.1752-1688.2009.00358.x

Rienzner, M., and Gandolfi, C. 2011. A composite statistical method for the detection of multiple undocumented abrupt changes in the mean value within a time series. *Int. J. Climatol.* **31**, 742-755. doi: 10.1002/joc.2113

Robinson, D.A., Dewey, K.F., and Heim, R.R. Jr. 1993. Global snow cover monitoring: An update. *Bull. Amer. Meteorol. Soc.,* **74**(9), 1689-1696. doi: 10.1175/1520-0477(1993)074<1689:GSCMAU>2.0.CO;2

Robinson, D.A., Estilow, T.W., and NOAA CDR Program (2012): NOAA Climate Data Record (CDR) of Northern Hemisphere (NH) Snow Cover Extent (SCE), Version 1. NOAA National Centers for Environmental Information. doi: 10.7289/V5N014G9 [February 18, 2019].

Ruddell, D., Hoffman, D., Ahmad, O., and Brazel, A.J. 2013. Historical threshold temperatures for Phoenix (urban) and Gila Bend (desert), central Arizona, USA. *Clim. Res.* **55**, 201-215. doi: 10.3354/cr01130

Ruggieri, E. 2013. A Bayesian approach to detecting change points in climatic records. *Int. J. Climatol.* **33**, 520-528. doi: 10.1002/joc.3447

Runnalls, K.E., and Oke, T.R. 2006. A technique to detect microclimatic inhomogenieties in historical records of screen-level air temperature. *J. Climate* **19**(6), 959-978. doi: 10.1175/JCLI3663.1

Santana, R., and Coelho, R. 2012. Low-frequency ambient noise generator with application to automatic speaker classification. *EURASIP J. Adv. Signal Process.* **2012**, 175.

Schroeder, M. 1991. *Fractals, Chaos, Power Laws: Minutes from an Infinite Paradise*. W.H. Freeman & Co., New York, 429pp. ISBN13: 9780716723578

Seidel, D.J., and Lanzante, J.R. 2004. An assessment of three alternatives to linear trends for characterizing global atmospheric temperature changes. *J. Geophys. Res. Atmos.* **109**(D14108). doi: 10.1029/2003JD004414

Sen, P.K. 1965. Some non-parametric tests for *m*-dependent time series. *J. Am. Stat. Assoc.* **60**(309), 134-147. doi: 10.2307/2283141

Shao, X., and Zhang, X. 2010. Testing for change points in time series. *J. Am. Stat. Assoc.* **105**(491), 1228-1240. doi: 10.1198/jasa.2010.tm10103

Streletskiy, D.A., Shiklomanov, N.I., Nelson, F.E., and Klene, A.E. 2008. Thirteen years of observations at Alaskan CALM sites: Long-term active layer and ground surface temperature trends. *9th International Conference on Permafrost*, 1727-1732.

Sutcliffe, J., Hurst, S., Awadallah, A.G., Brown, E., and Hamed, K. 2016. Harold Edwin Hurst: the Nile and Egypt, past and future. *Hydrolog. Sci. J.* **61**(9), 1557-1570. doi: 10.1080/02626667.2015.1019508

Swanson, K.L., and Tsonis, A.A. (2009). Has the climate recently shifted? *Geophys. Res. Lett.* **36**(L06711). doi: 10.1029/2008GL037022

Tan, X., and Gan, T.Y. 2017. Multifractality of Canadian precipitation and streamflow. *Int. J. Climatol.* **37**(S1), 1221-1236. doi: 10.1002/joc/5078

Tharu, B., and Dhakal, N. 2020. On the use of Bayesian quantile regression method to explore the historical trends in extreme precipitation and their connections with large-scale climate patterns over the contiguous USA. *Theor. Appl. Climatol.* **139**, 1277-1290. doi: 10.1007/s00704-019-03054-w

Todhunter, P.E. 2012. Uncertainty of the assumptions required for estimating the regulatory flood: Red River of the North. *J. Hydrol. Eng.* **17**, 1011-1020. doi: 10.1061/(ASCE)HE.1943-5584.0000560

Todhunter, P.E., and Fietzek-DeVries, R. 2016. Natural hydroclimatic forcing of historical lake volume fluctuations at Devils Lake, North Dakota (USA). *Nat. Hazards* **81**, 1515-1532. doi: 10.1007/s11069-015-2143-6

Treeflow. 2019. Website at https://www.treeflow.info, accessed on June 10, 2019.

van Atta, C.W., and Helland, K.N. 1977. A note on the Hurst phenomenon in turbulent flows. *Water Resour. Res.* **13**(6), 1003-1005. doi: 10.1029/WR013I006P01003

van Loon, H., and Meehl, G.A. 2014. Interactions between externally forced climate signals from sunspot peaks and the internally generated Pacific Decadal and North Atlantic Oscillations. *Geophys. Res. Lett.* **41**, 161-166. doi: 10.1002/2013GL058670

Venrick, E.L., McGowan, J.A., Cayan, D.R., and Hayward, T.L. 1987. Climate and chlorophyll a: Long-term trends in the central North Pacific Ocean. *Science* **238**(4823), 70-72. doi: 10.1126/science.238.4823.70

Wallis, J.R., and O'Connell P.E. 1973. Firm reservoir yield – How reliable are historic hydrological records? *Hydrol. Sci. B.* **18**(3), 347-365. doi: 10.1080/02626667309494046

Wasserstein, R.L., Schirm, A.L., and Lazar, N.A. 2019. Moving to a world beyond "$p < 0.05$." *Am. Stat.* **73**(Sup 1), 1-19. doi: 10.1080/00031305.2019.1583913

Weatherhead, E.C., Reinsel, G.C., Tiao, G.C., *et al.* 1998. Factors affecting the detection of trends: Statistical considerations and applications to environmental data. *J. Geophys. Res.* **103**, 17149-17161. doi: 10.1029/98JD00995

Wu, Q., Xie, X.-Q., Mei, Y., and He, W.-P. 2021. A new early warning indicator of abrupt climate change based on the changing normalized dynamic range. *Int. J. Climatol.* **41**, 2983-2995. doi: 10.1002/joc.7000

Xie, H., Li, D., and Xiong, L. 2014. Exploring the ability of the Pettitt method for detecting change point by Monte Carlo simulation. *Stoch. Environ. Res. Risk Assess* **28**, 1643-1655. doi: 10.1007/s00477-013-0814-y

Xie, X.-Q., He, W.-P., Gu, B., Mei, Y., and Zhao, S.S. 2019. Can kurtosis be an early warning signal for abrupt climate change? *Clim. Dyn.* **52**(11), 6863-6876. doi: 10.1007/s00382-018-4549-9

Xie, Y., Huang, J., and Willett, R. 2013. Change-point detection for high-dimensional time series with missing data. *IEEE J. Sel. Topics Signal Process.* **7**(1), 12-27. doi: 10.1109/JSTSP.2012.2234082

Xiong, L., and Guo, S. 2004. Trend test and change-point detection for the annual discharge series of the Yangtze River at the Yichang hydrological station. *Hydrol. Sci. J.* **49**(1), 99-112. doi: 10.1623/hysj.49.1.99.53998

You, C., Lin, D.K.J., and Young, S.S. 2018. Time series smoother for effect detection. *PLOS ONE* **13**, e0195360. doi: 10.1371/journal.pone.0195360

Yu, M., and Ruggieri, E. 2019. Change point analysis of global temperature records. *Int. J. Climatol.* **39**, 3679-3688. doi: 10.1002/joc.6042

Yue, S., Pilon, P., and Cavadias, G.S. 2002. Power of the Mann-Kendall and Spearman's rho tests for detecting monotonic trends in hydrological series. *J. Hydrol.* **259,** 254-271. doi: 10.1016/S0022-1694(01)00594-7

Zhang, Y., Wallace, J.M., and Battisti, D.S. 1997. ENSO-like interdecadal variability: 1900-93. *J. Climate* **10**(5), 1004-1020. doi: 10.1175/1520-0442(1997)010<1004:ELIV>2.0.CO;2

Zhou, C., van Nooijen, R., Kolechkina, A., and Hrachowitz, M. 2019. Comparative analysis of nonparametric change-point detectors commonly used in hydrology. *Hydrol. Sci. J.* **64**(14), 1690-1710. doi: 10.1080/02626667.2019.1669792

Zhou, H., and Liu, Y. 2018: Spatio-temporal pattern of meteorological droughts and its possible linkage with climate variability. *Int. J. Climatol.* **38**, 2082-2096. doi: 10.1002/joc.5319

**Table 1:** Simple example of a dataset with discontinuities. The observations ($X_t$) are taken from a Gaussian normal distribution that are $N(20,2)$ for $t = 1,15$, $N(22,2)$ for $t = 16,34$, and $N(22,4)$ for $t = 35,50$. Data are rounded to two decimal places.

| $t$ | $X_t$ | $X_t - \bar{X}$ | Running Sum of Mean Deviations | Normalized Rescaled Running Sum | | $t$ | $X_t$ | $X_t - \bar{X}$ | Running Sum of Mean Deviations | Normalized Rescaled Running Sum |
|---|---|---|---|---|---|---|---|---|---|---|
| 1 | 21.52 | -0.55 | -0.55 | 0.99 | | 26 | 21.69 | -0.38 | -39.04 | 0.14 |
| 2 | 19.79 | -2.28 | -2.83 | 0.94 | | 27 | 28.28 | 6.21 | -32.83 | 0.27 |
| 3 | 16.78 | -5.29 | -8.13 | 0.82 | | 28 | 24.34 | 2.27 | -30.56 | 0.32 |
| 4 | 17.40 | -4.67 | -12.80 | 0.72 | | 29 | 18.37 | -3.70 | -34.26 | 0.24 |
| 5 | 19.83 | -2.24 | -15.05 | 0.67 | | 30 | 20.84 | -1.23 | -35.50 | 0.21 |
| 6 | 17.87 | -4.20 | -19.25 | 0.57 | | 31 | 23.27 | 1.20 | -34.30 | 0.24 |
| 7 | 19.52 | -2.55 | -21.81 | 0.52 | | 32 | 19.73 | -2.34 | -36.65 | 0.19 |
| 8 | 21.02 | -1.05 | -22.86 | 0.49 | | 33 | 21.04 | -1.03 | -37.69 | 0.17 |
| 9 | 16.93 | -5.14 | -28.01 | 0.38 | | 34 | 19.65 | -2.42 | -40.11 | 0.11 |
| 10 | 21.35 | -0.72 | -28.73 | 0.36 | | 35 | 18.59 | -3.48 | -43.59 | 0.04 |
| 11 | 20.00 | -2.07 | -30.80 | 0.32 | | 36 | 20.46 | -1.61 | -45.21 | 0.00 |
| 12 | 21.43 | -0.64 | -31.44 | 0.30 | | 37 | 31.37 | 9.30 | -35.91 | 0.21 |
| 13 | 17.63 | -4.44 | -35.88 | 0.21 | | 38 | 32.83 | 10.76 | -25.15 | 0.44 |
| 14 | 23.07 | 1.00 | -34.89 | 0.23 | | 39 | 21.88 | -0.19 | -25.35 | 0.44 |
| 15 | 20.46 | -1.67 | -36.50 | 0.19 | | 40 | 28.19 | 6.12 | -19.24 | 0.57 |
| 16 | 19.38 | -2.69 | -39.19 | 0.13 | | 41 | 22.07 | 0.00 | -19.24 | 0.57 |
| 17 | 23.85 | 1.78 | -37.42 | 0.17 | | 42 | 26.96 | 4.89 | -14.35 | 0.68 |
| 18 | 21.41 | -0.66 | -38.08 | 0.16 | | 43 | 21.80 | -0.27 | -14.62 | 0.68 |
| 19 | 24.84 | 2.77 | -35.31 | 0.22 | | 44 | 27.21 | 5.14 | -9.49 | 0.79 |
| 20 | 21.02 | -1.05 | -36.36 | 0.20 | | 45 | 18.27 | -3.80 | -13.29 | 0.71 |
| 21 | 25.40 | 3.33 | -33.04 | 0.27 | | 46 | 25.59 | 3.52 | -9.77 | 0.78 |
| 22 | 15.38 | -6.69 | -39.72 | 0.12 | | 47 | 22.43 | 0.36 | -9.41 | 0.79 |
| 23 | 23.74 | 1.67 | -38.06 | 0.16 | | 48 | 21.58 | -0.49 | -9.91 | 0.78 |
| 24 | 23.25 | 1.18 | -36.88 | 0.18 | | 49 | 21.95 | -0.12 | -10.03 | 0.78 |
| 25 | 20.30 | -1.77 | -38.65 | 0.14 | | 50 | 32.10 | 10.03 | 0.00 | 1.00 |

| | | | |
|---|---|---|---|
| Grand Maximum: | 32.83 | Grand Minimum: | 15.38 |
| Grand Mean: | 22.07 | Standard Deviation: | 3.86 |
| Range: | 17.45 | Rescaled Range: | 11.72 |

Hurst Exponent: 0.6292

**Figure 1:** Time series of Northern Hemisphere air temperature from Moberg *et al.* (2005) (top) and a simulated "climate" having the same variance as the Moberg *et al.* time series but generated from the average of twelve spins of a roulette wheel (bottom). Figure taken from Koutsoyiannis and Cohn (2008).

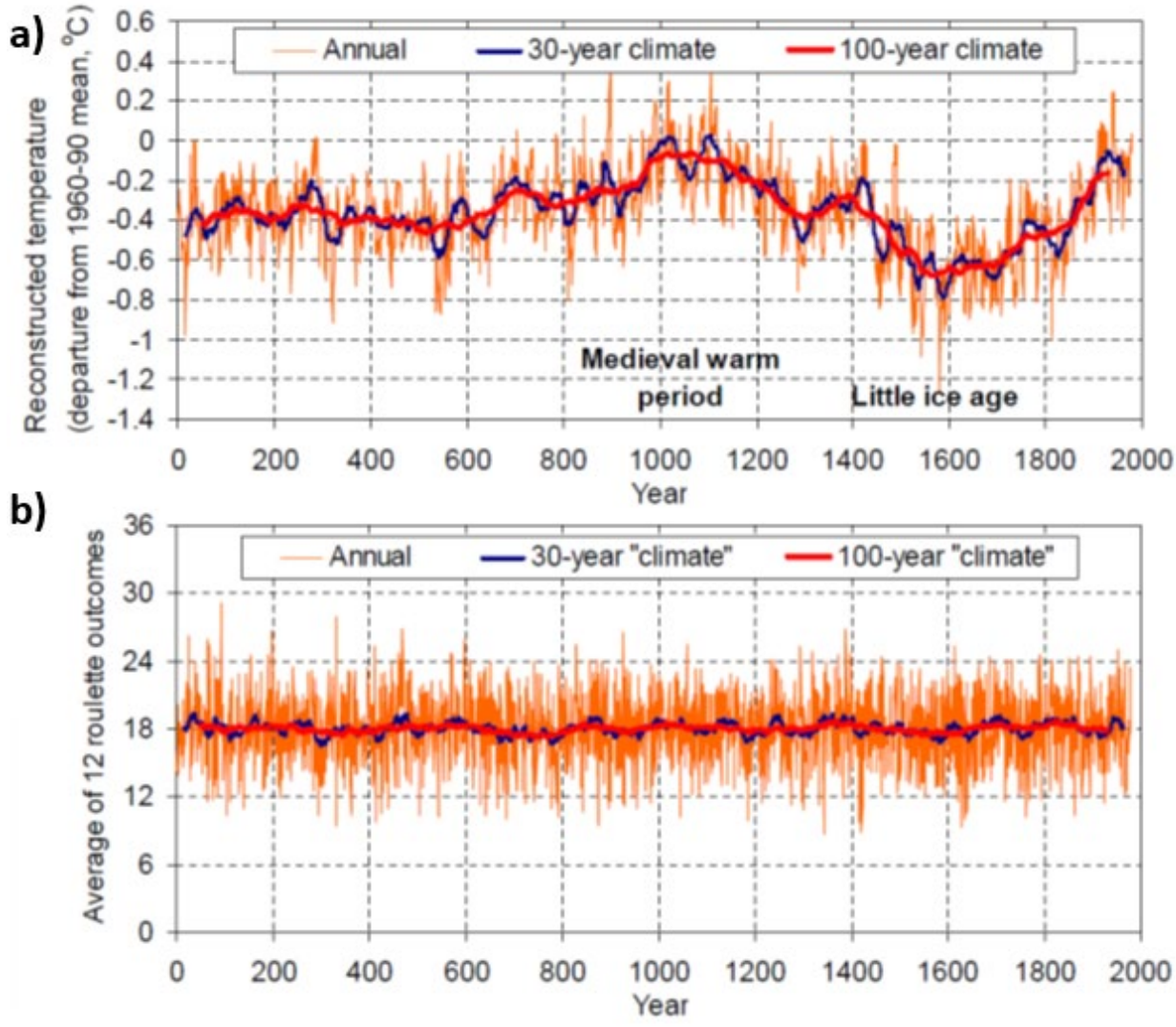

**Figure 2:** Raw observations from a hypothetical distribution (a) and its normalized rescaled running sum as a function of time (b).

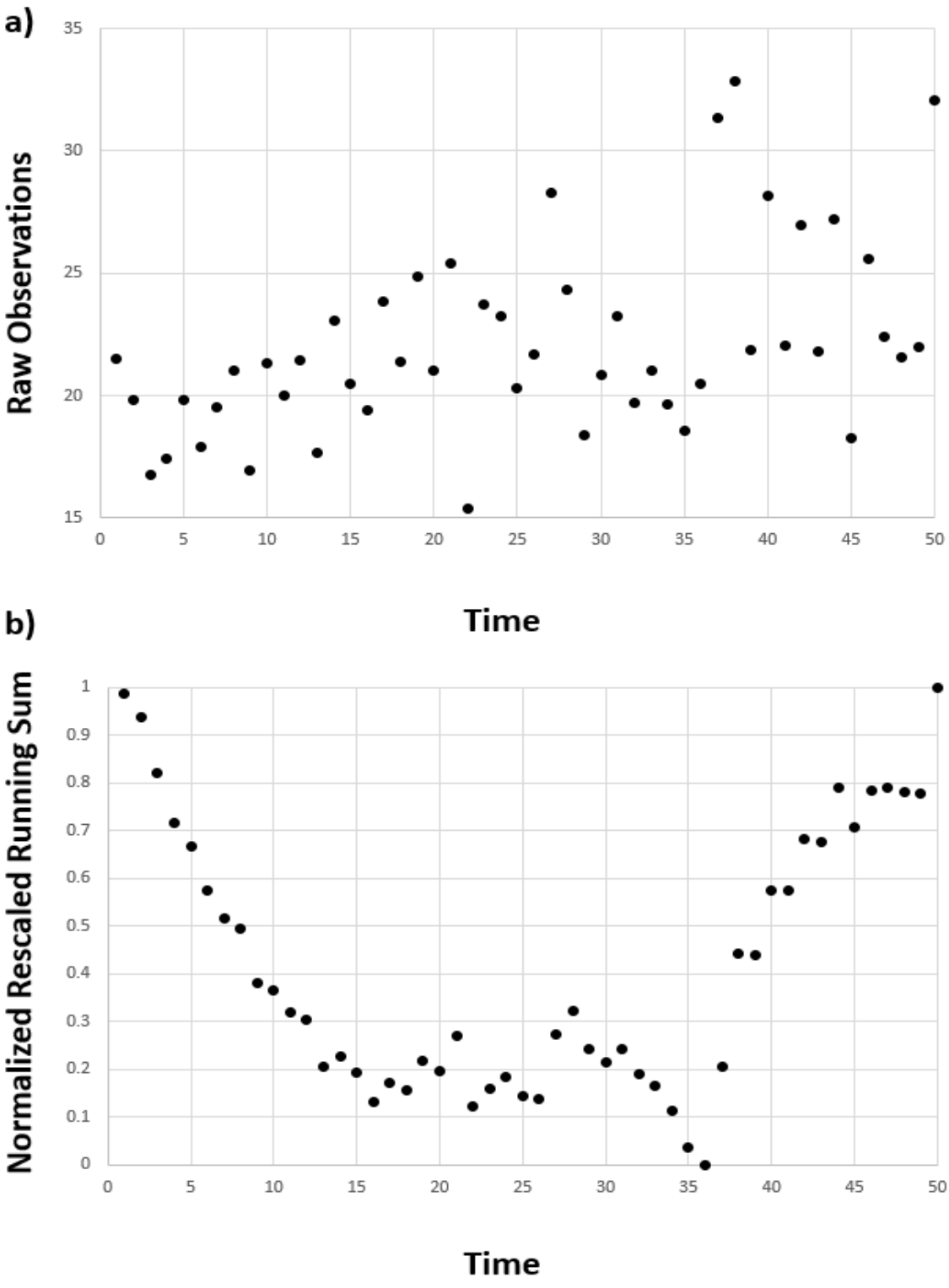

**Figure 3:** Monthly Pacific Decadal Oscillation (PDO from Nate Mantua) (a) and its normalized rescaled running sum as a function of time (b).

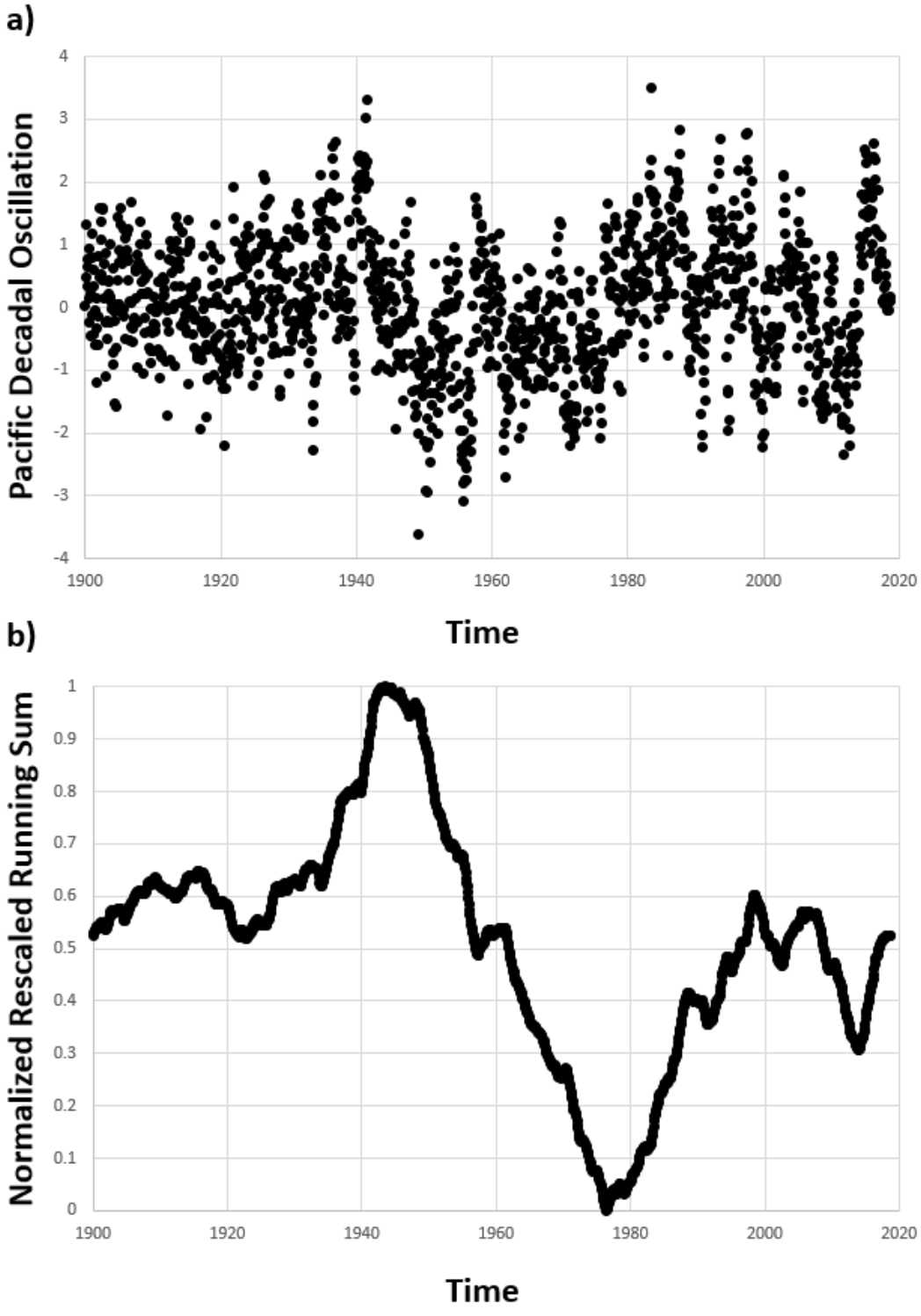

**Figure 4:** Thaw depths (in cm) for the four locations in northern Alaska (a) and their normalized rescaled running sum as a function of time (b).

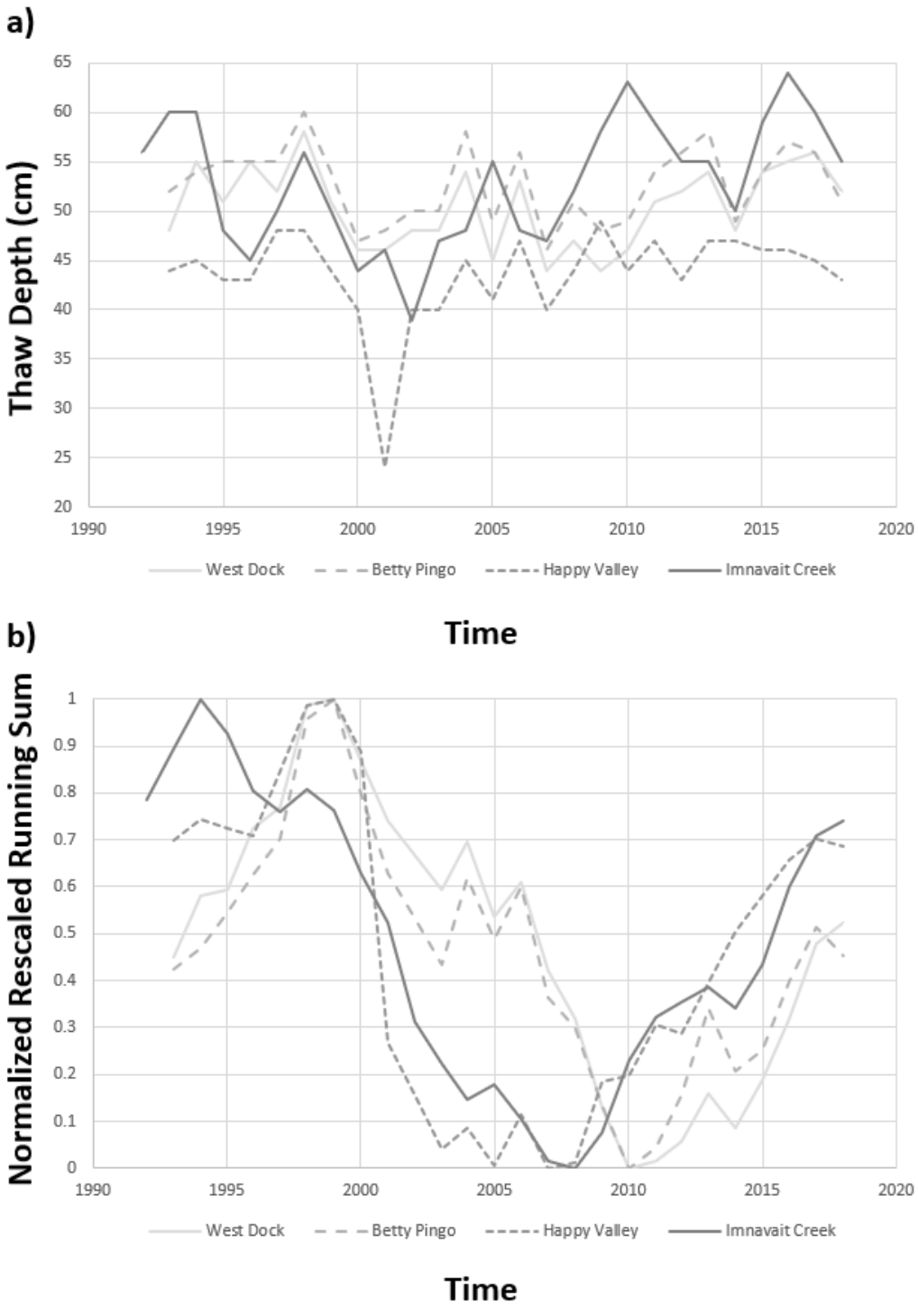

**Figure 5:** Maximum Northern Hemisphere snow cover extent (in $km^2$) (a) and its normalized rescaled running sum as a function of time (b).

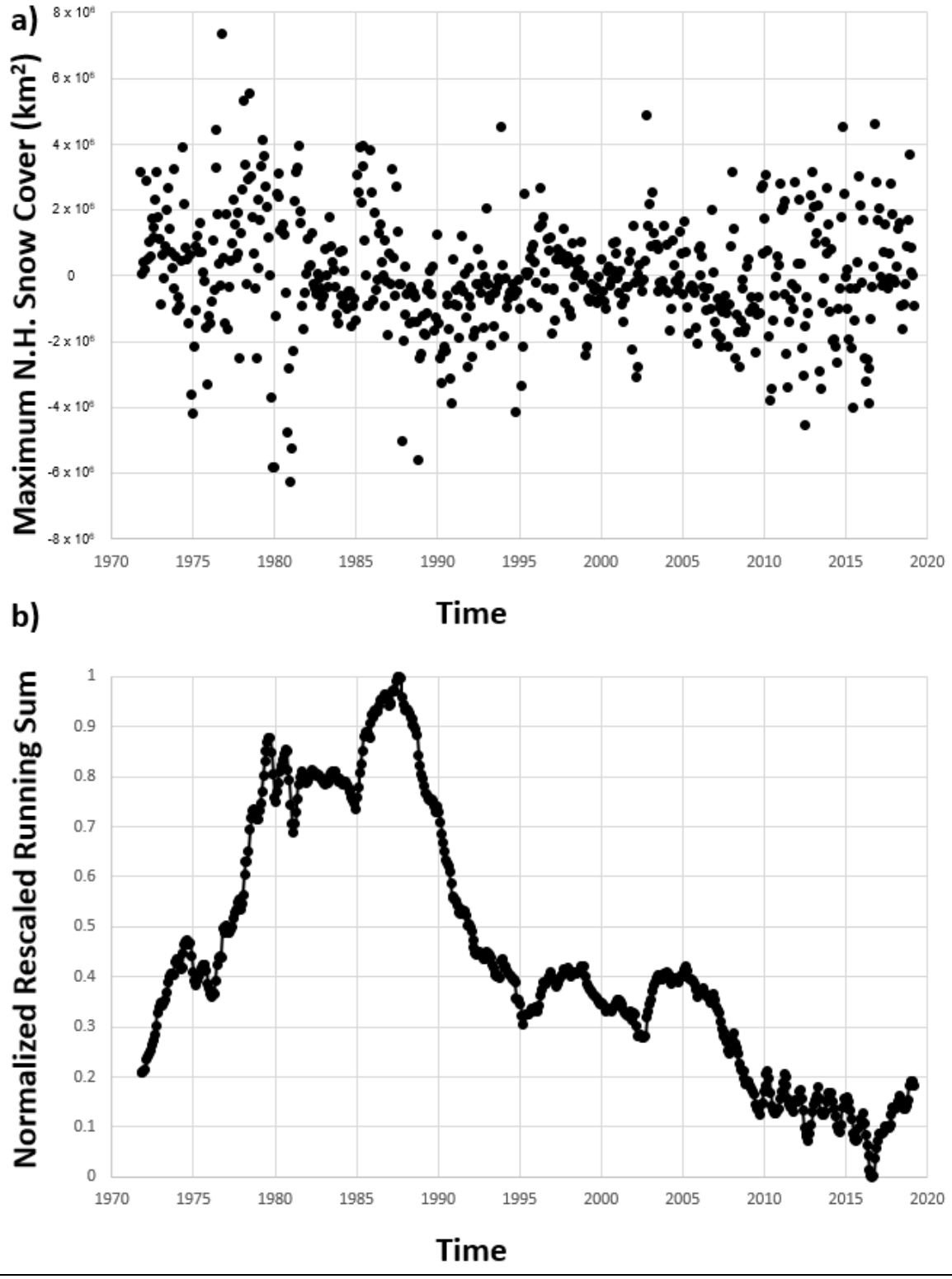

**Figure 6:** Maximum river flow (in $m^3 s^{-1}$) at Lees Ferry, Colorado (a) and its normalized rescaled running sum as a function of time for the entire period of record (b).

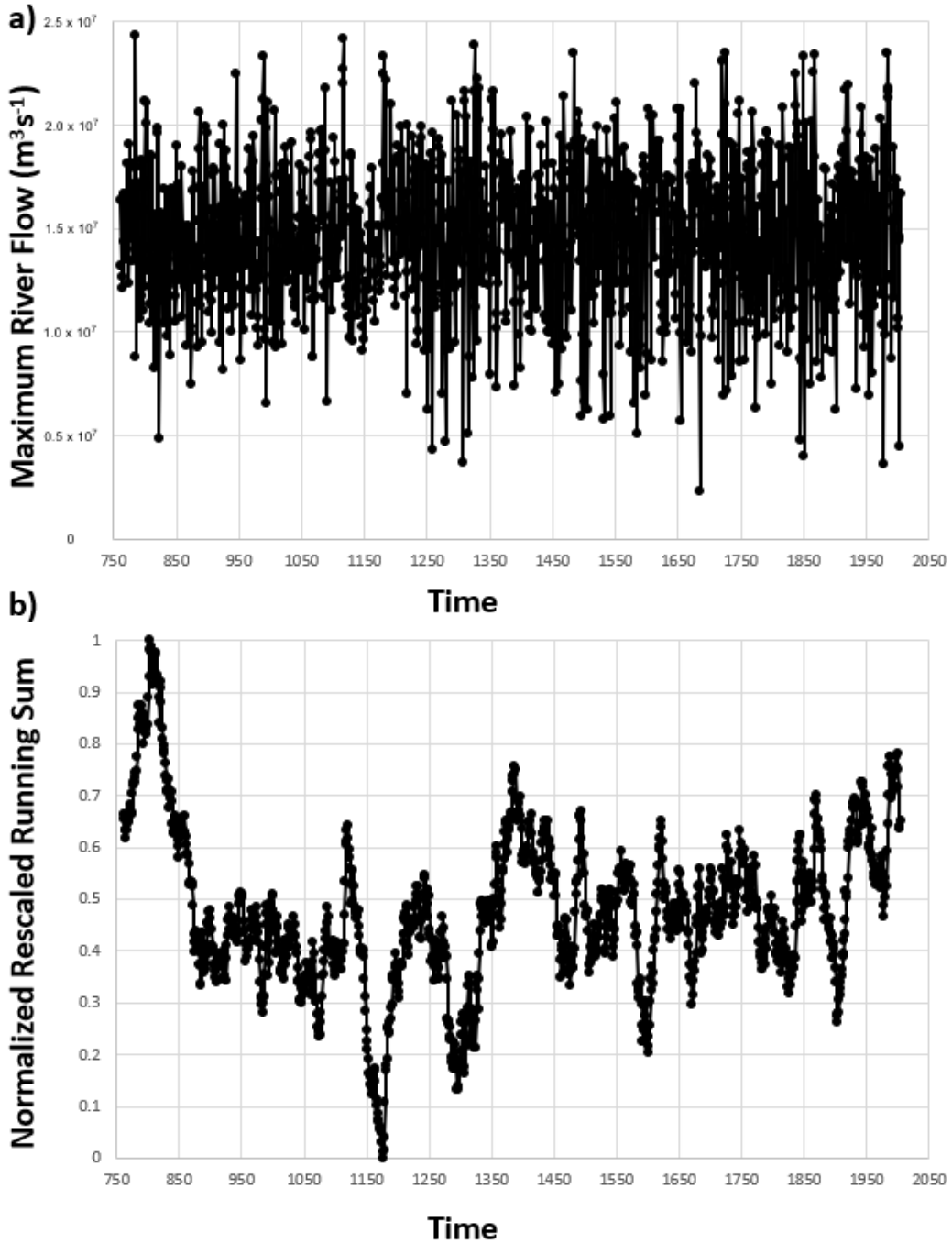

**Figure 7:** Total number of named storms (per year) in the North Atlantic basin (a) and its normalized rescaled running sum as a function of time (b).

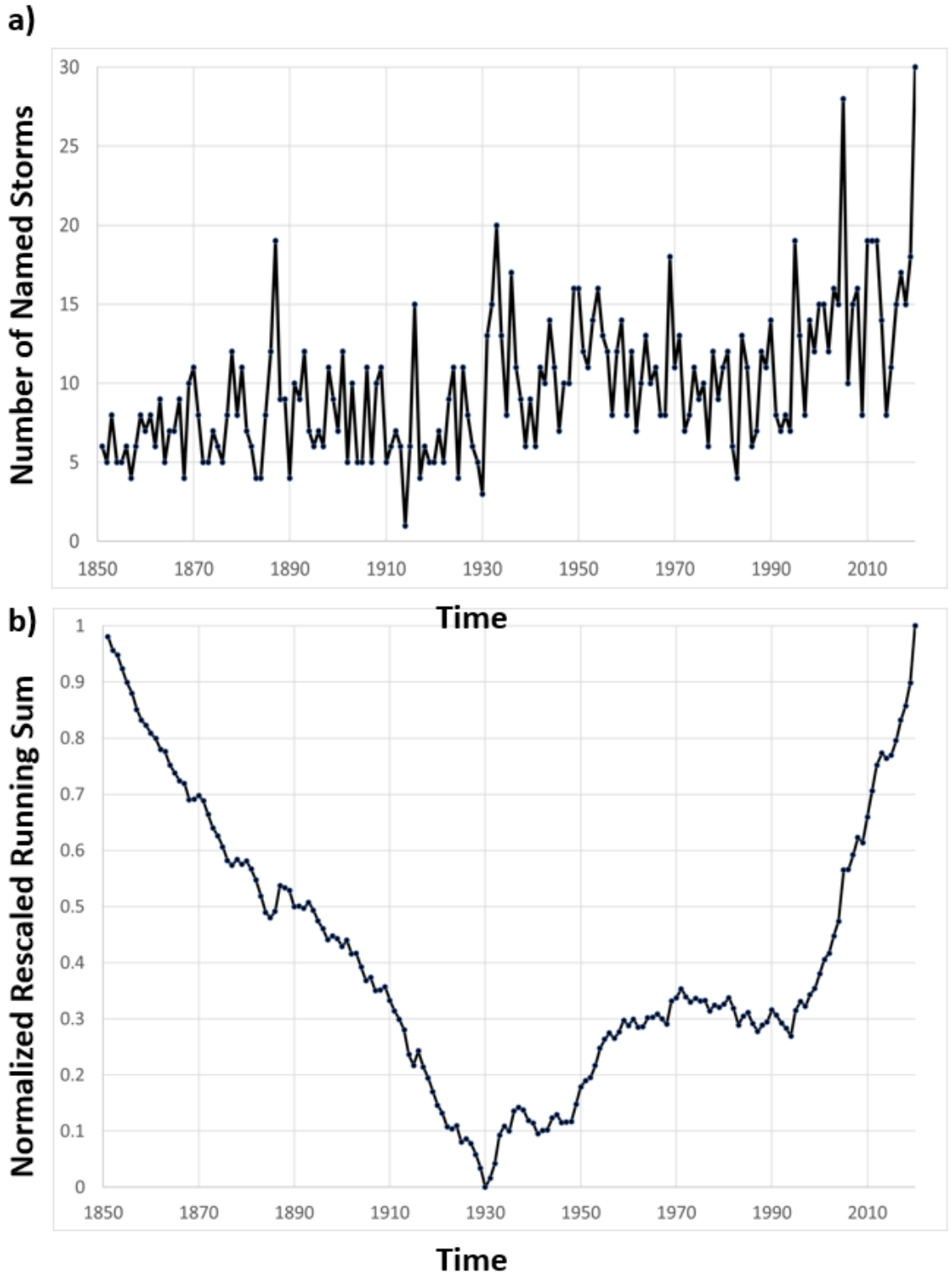

**Figure 8:** Central England air temperature (C°) (a) and its normalized rescaled running sum as a function of time (b).

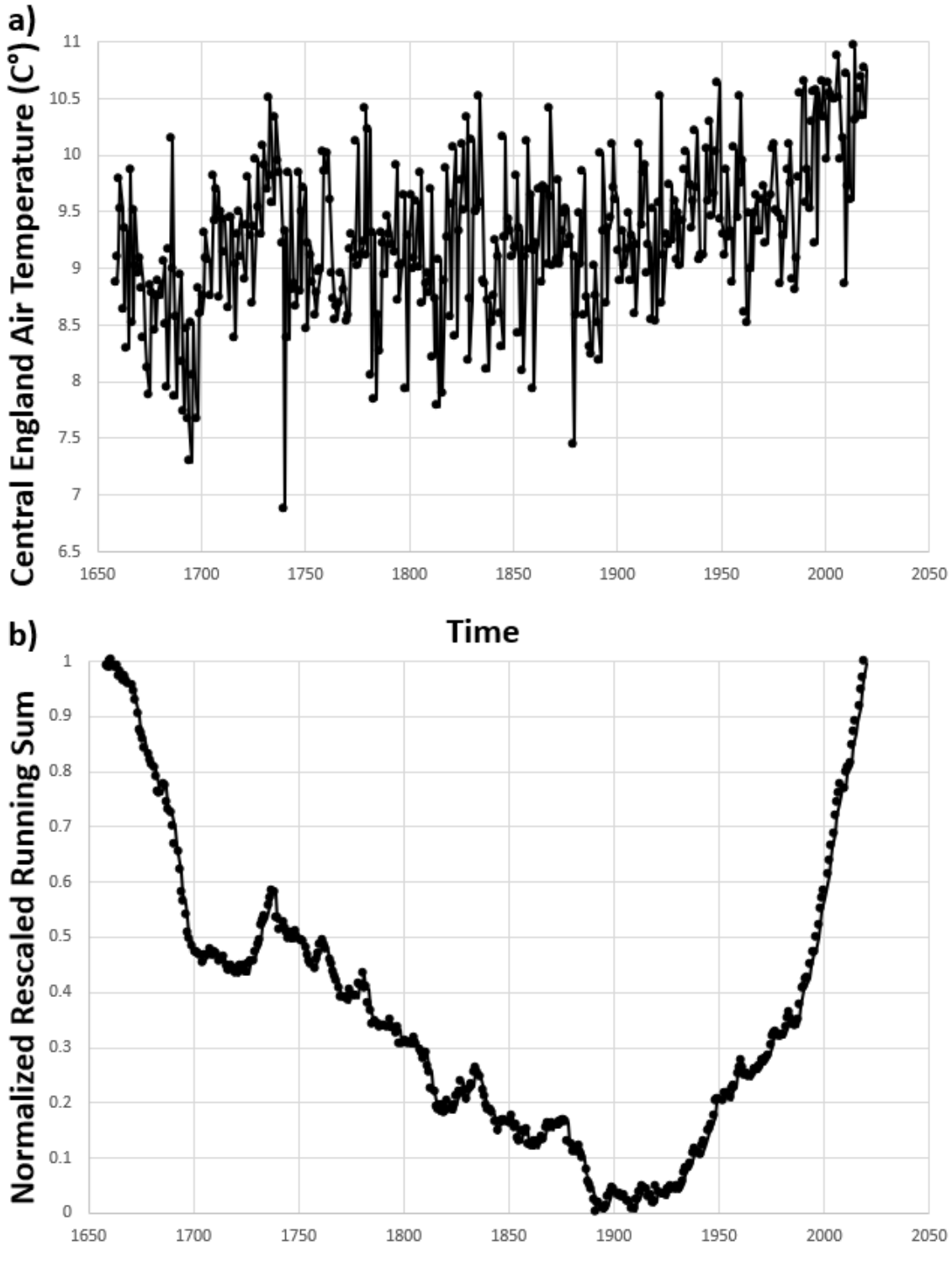

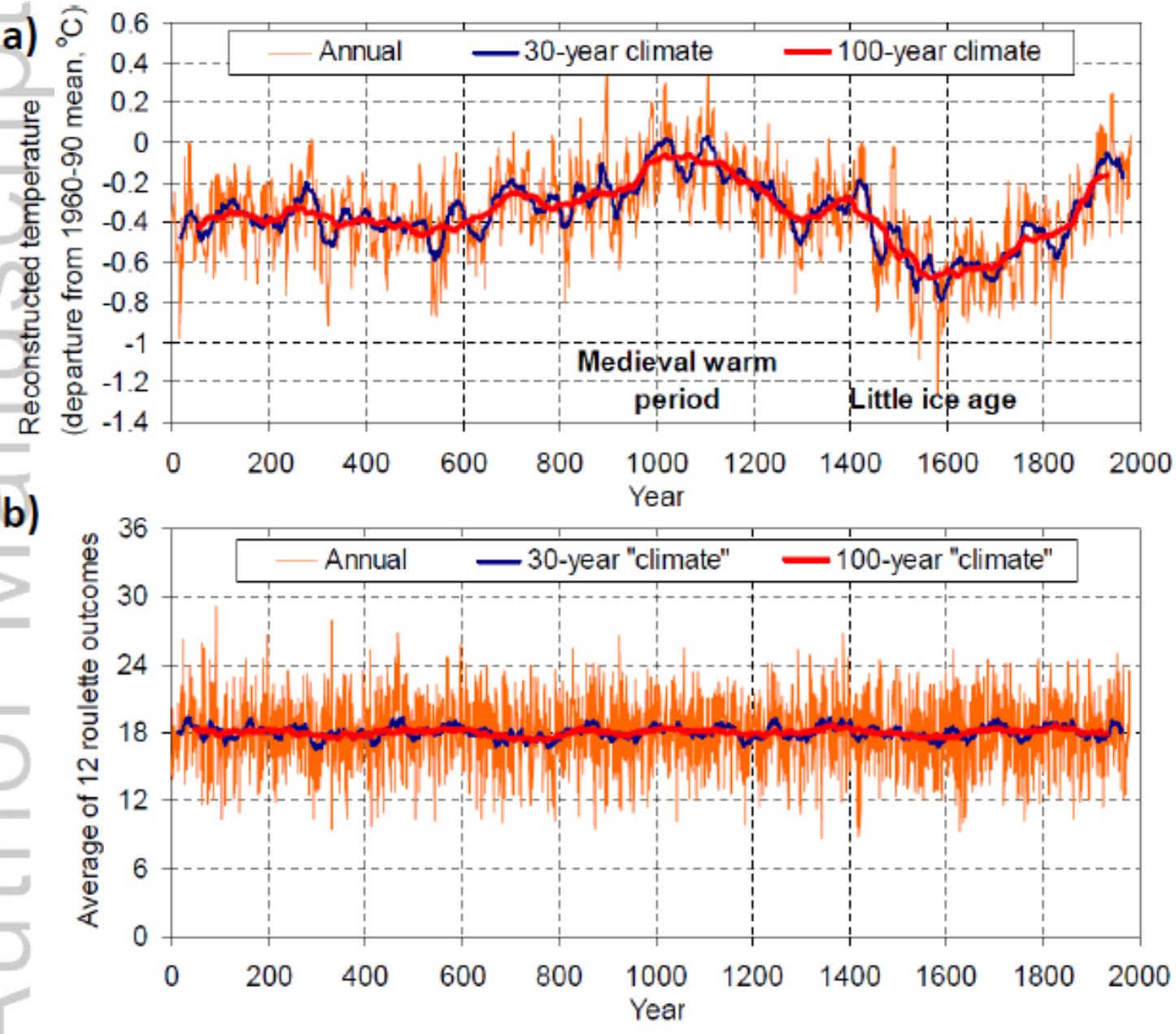


JOC_7502_Figure 1.tif

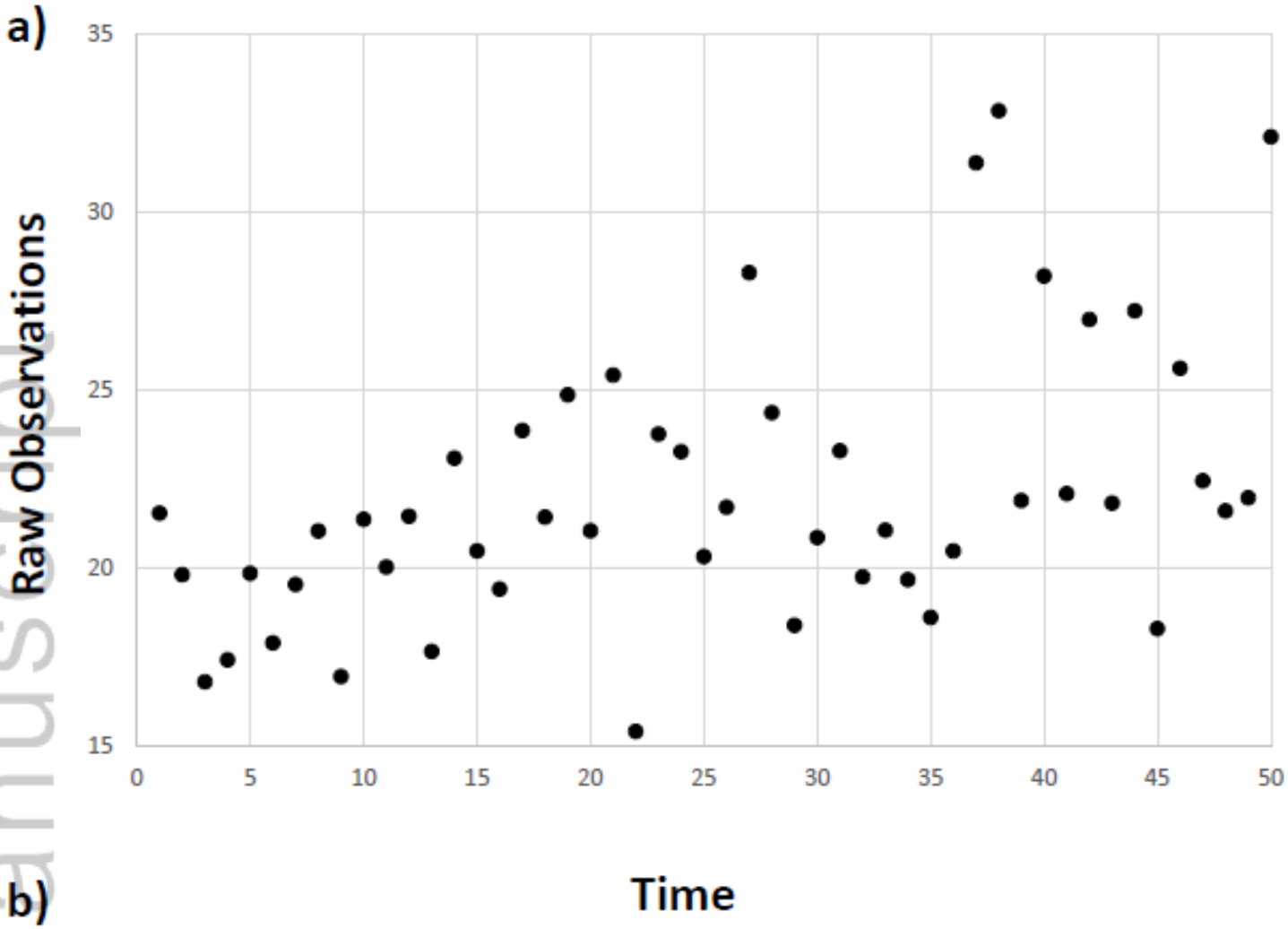


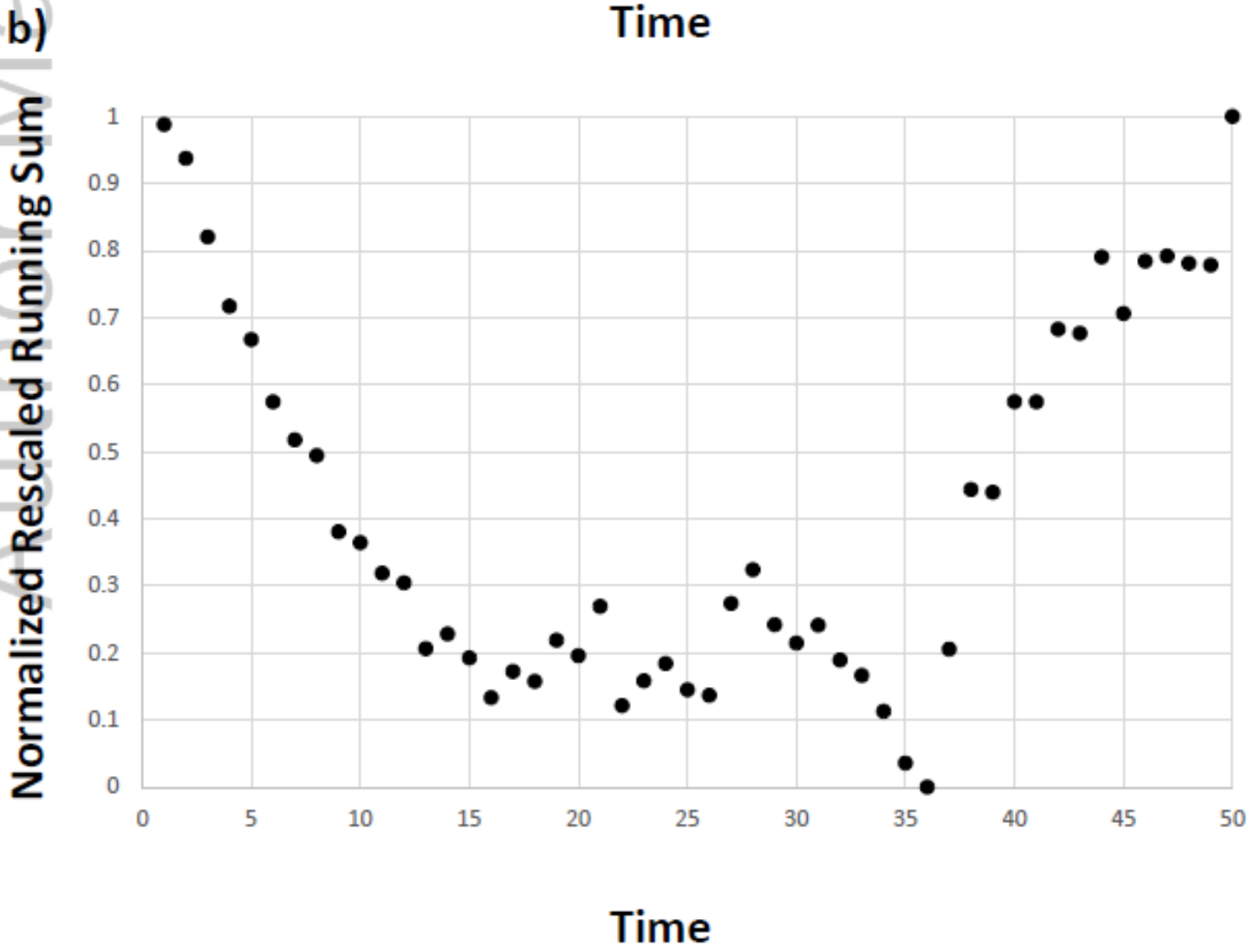


JOC 7502 Figure 2.tif

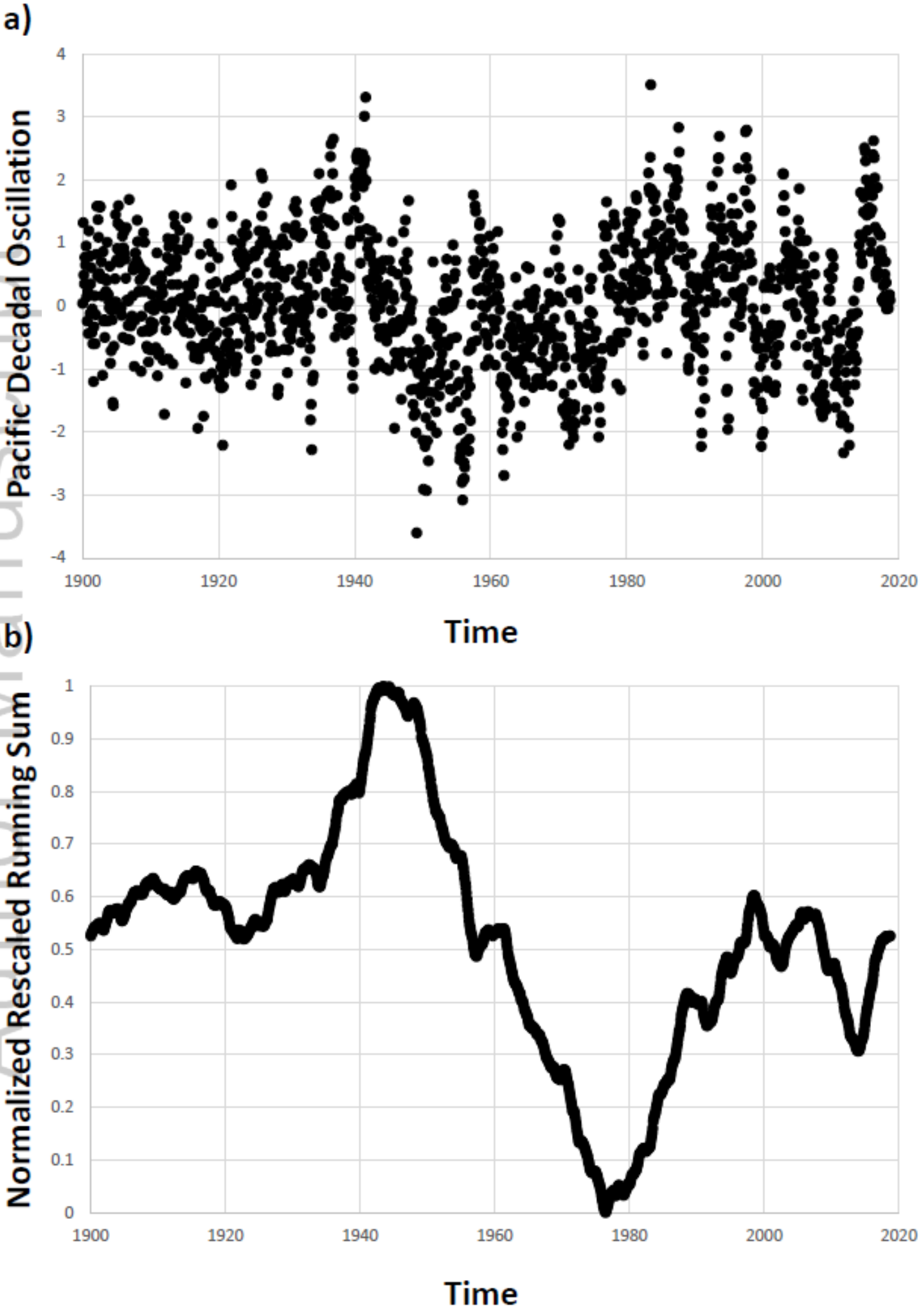

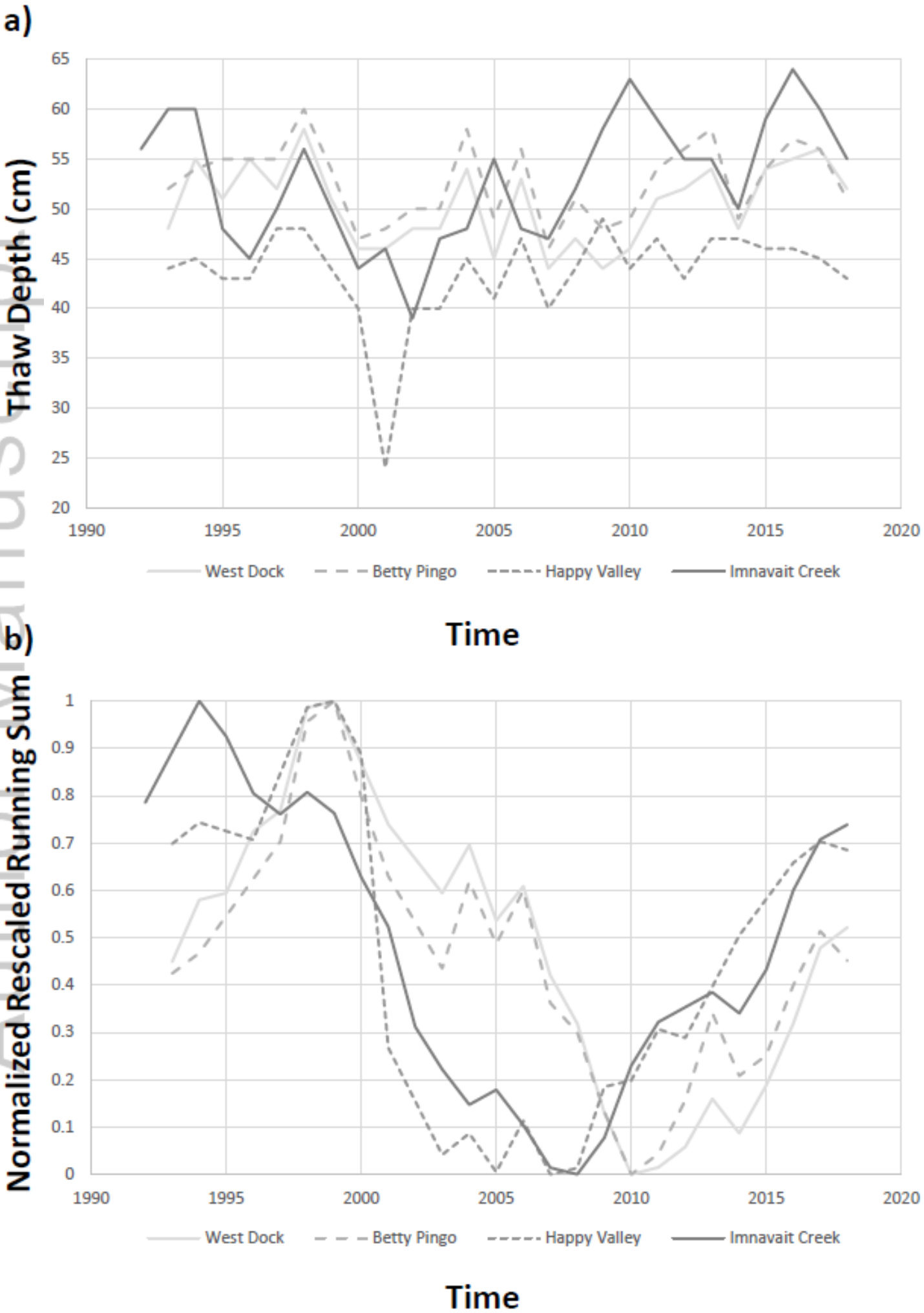




JOC_7502_Figure 4.tif

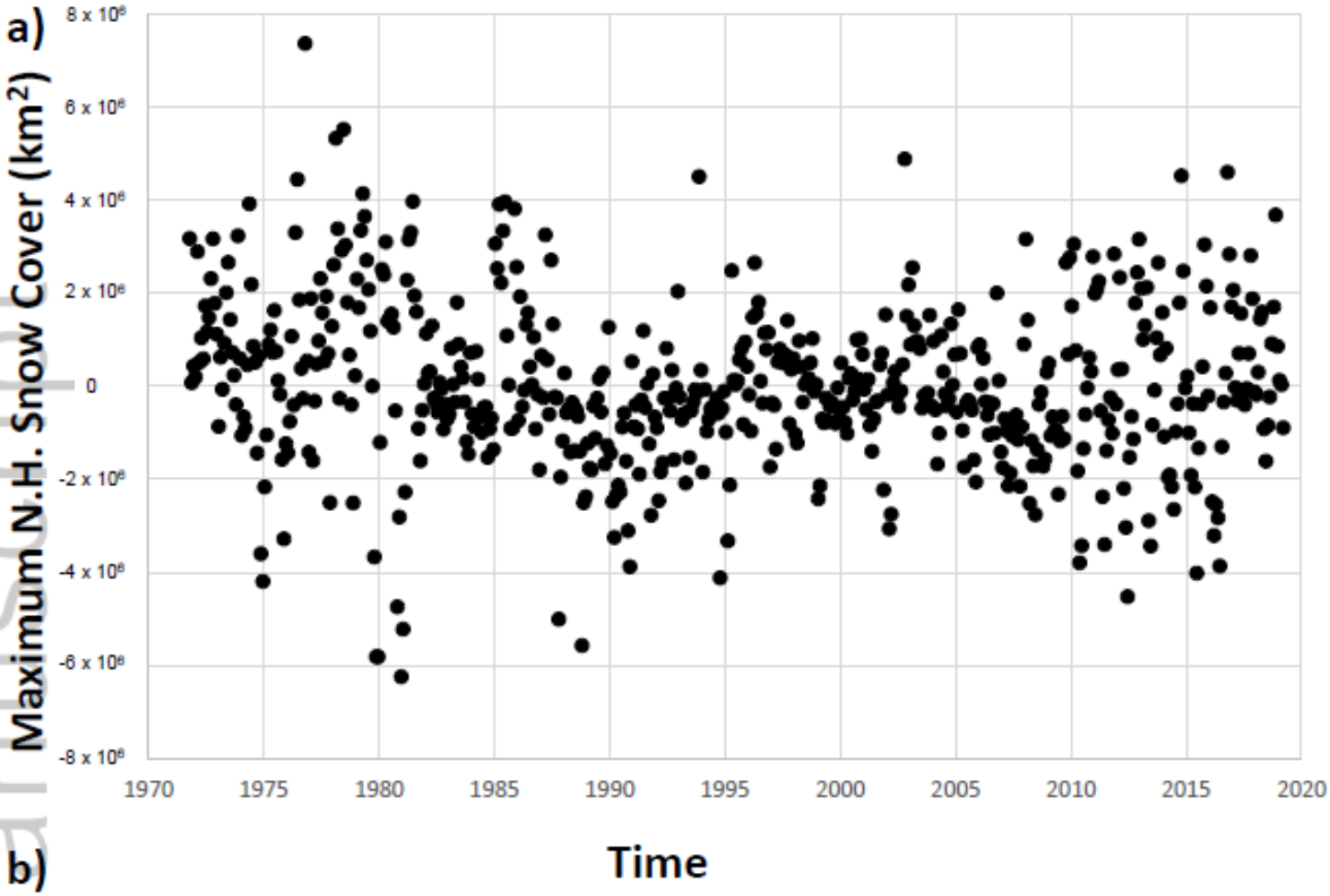


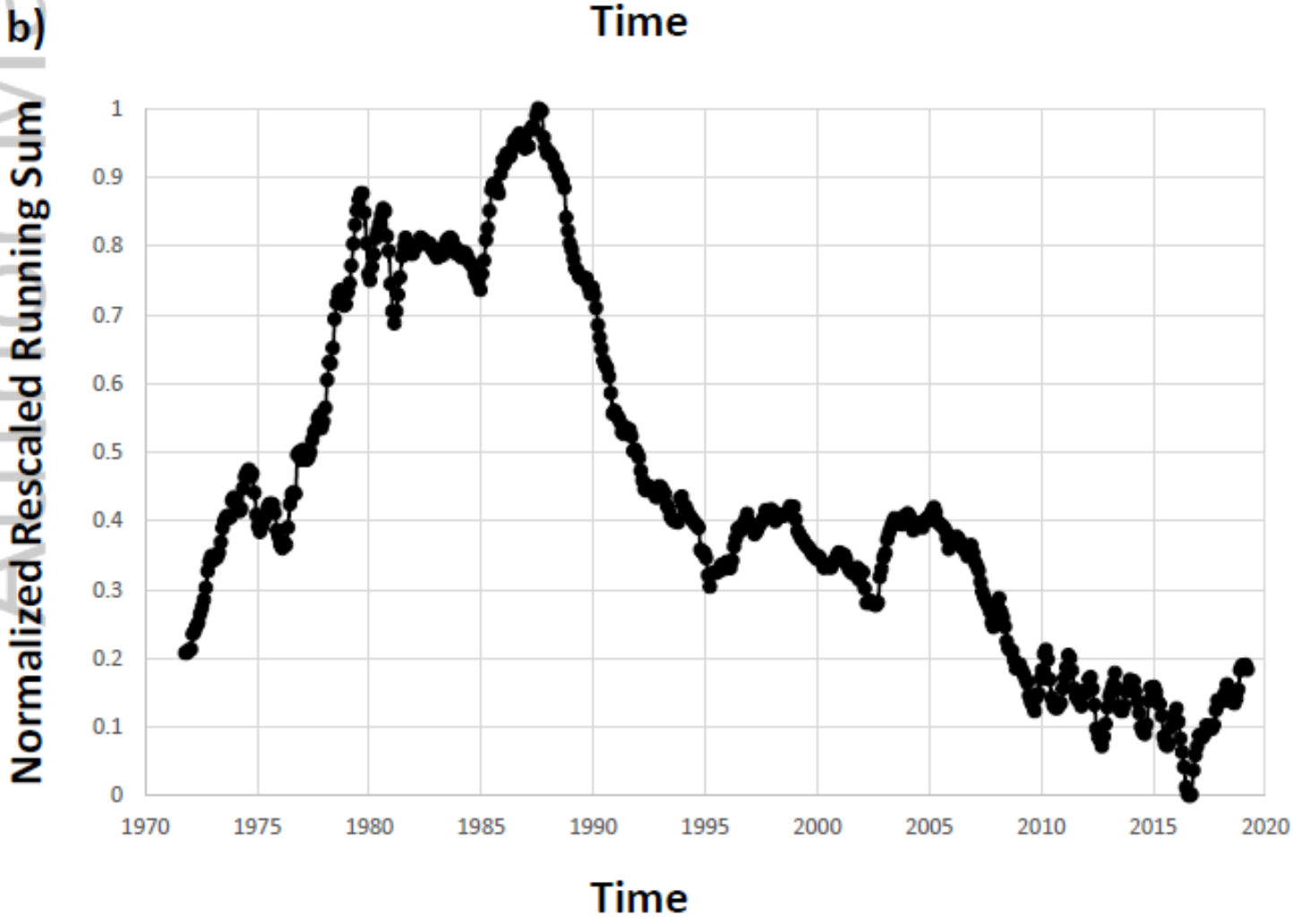


JOC_7502_Figure 5.tif

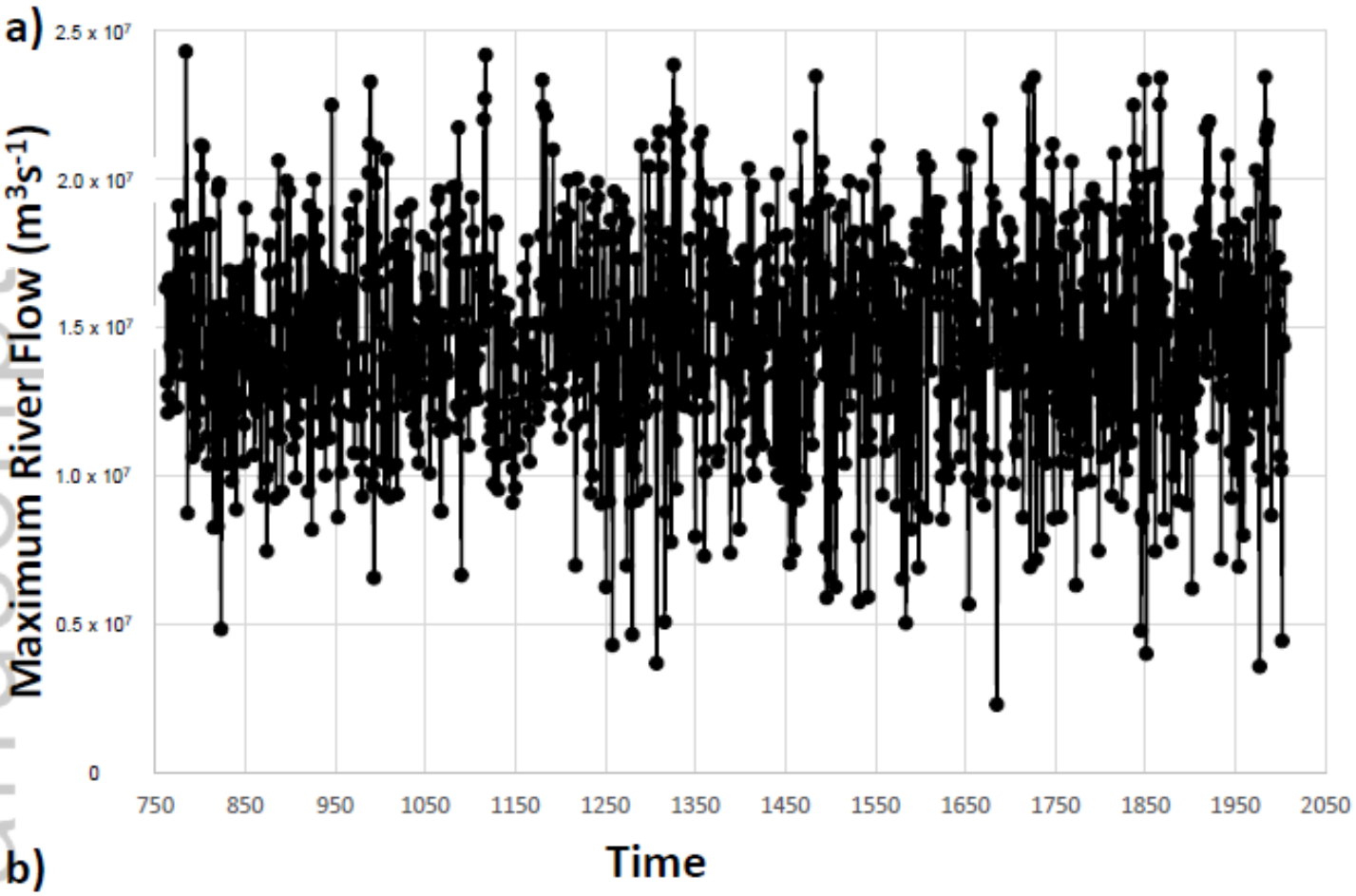


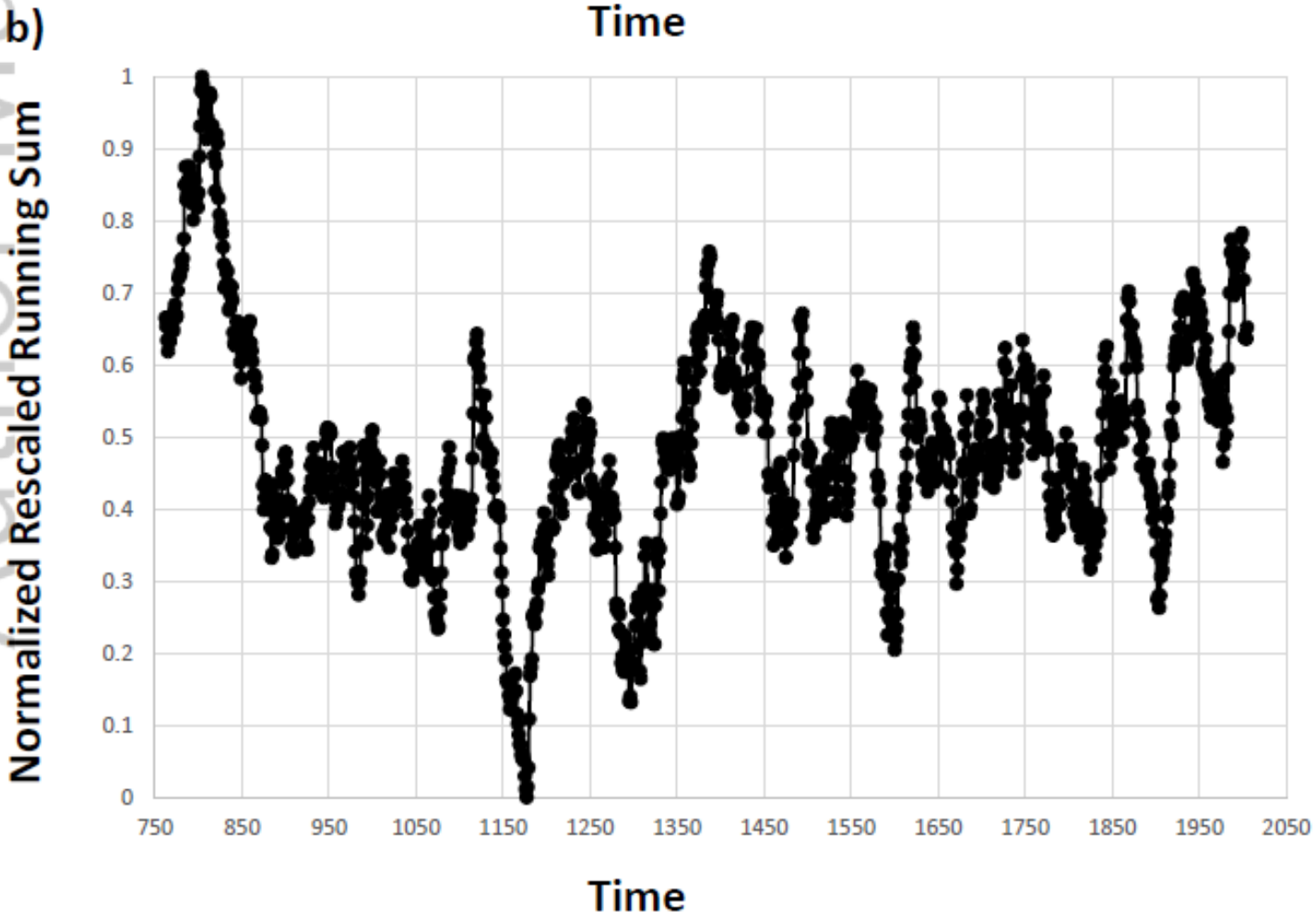


JOC_7502_Figure 6.tif

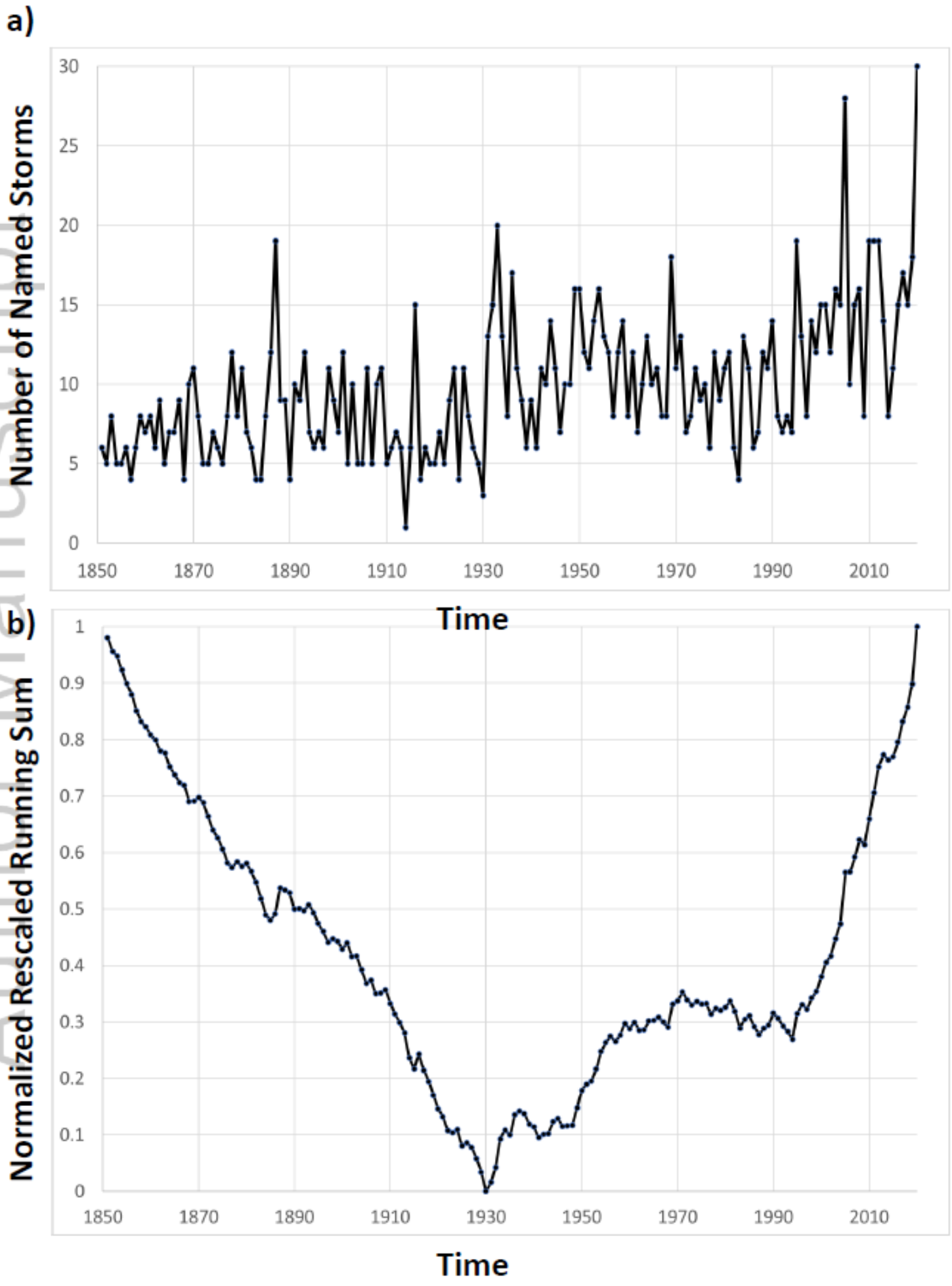


JOC_7502_Figure 7.tif

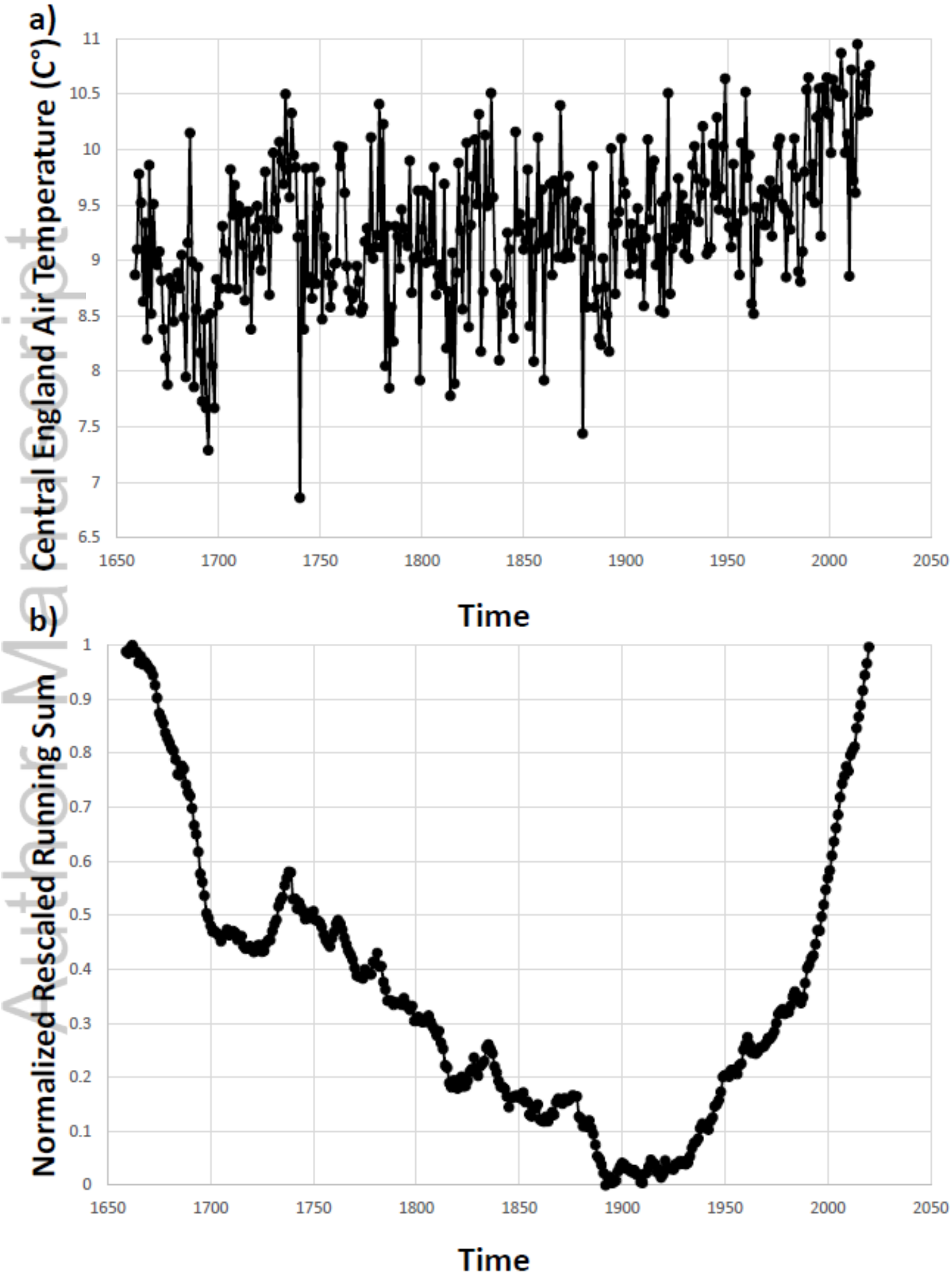


JOC_7502_Figure 8.tif

# Detection of Climate Transitions and Discontinuities

**David R. Legates and Samuel I. Outcalt**

The method of Outcalt *et al.* is reexamined to evaluate its efficacy in delineating changes in trends and identifying regime shifts in climatic-related time-series. It is based on the normalized rescaled running sum where temporal changes in the Hurst exponent identifies climatic trends from one regime to another. Examples focus on the Pacific Decadal Oscillation, Arctic thaw depth, the Northern Hemisphere snow cover extent, treeflow data from Lee's Ferry, North Atlantic named storm frequency, and central England air temperatures.